Sustainable Food Technology

ROYAL SOCIETY OF CHEMISTRY

PAPER

View Article Online
View Journal

Cite this: DOI: 10.1039/d5fb00546a

Integrated performance assessment of vacuum heat pump drying: a multi-criteria framework for energy-quality optimization in banana slice drying

Thanapon Saengsuwan [a] and Narathip Sujinda *[b]

The industry faces significant challenges from growing demands for energy-efficient food processing while maintaining exceptional product quality has created significant challenges for the industry. An integrated performance assessment framework for vacuum heat pump drying (VHPD) systems was developed in this study, combining thermodynamic analysis with comprehensive quality evaluation through multi-criteria optimization. Banana slices were dried using a laboratory-scale VHPD system at temperatures ranging from 40–60 °C and vacuum pressures of 0–80 kPa. Six thin-layer drying models were evaluated, with the Page model exhibiting superior predictive performance (R^2 = 0.9964, RMSE = 0.0150). Effective moisture diffusivity was found to range from 1.15 × 10^{-10} to 1.98 × 10^{-10} m^2 s^{-1}, with activation energies between 16.47–19.60 kJ mol^{-1}. A novel Integrated Performance Index (IPI) was constructed incorporating a specific moisture extraction rate, exergy efficiency, color retention, and vitamin C preservation using multi-criteria decision analysis. Optimal conditions (60 °C, 80 kPa) were identified, achieving an IPI of 0.796 while balancing efficiency (SMER = 0.179 kg water per kWh, exergy efficiency = 0.524) with quality retention (vitamin C = 46.6%). Response surface analysis was subsequently employed to identify robust optimization regions for practical implementation. This framework represents the first comprehensive approach unifying energy, exergy, and quality parameters within a single decision-support tool for sustainable food processing.

Received 1st September 2025
Accepted 28th October 2025

DOI: 10.1039/d5fb00546a

rsc.li/susfoodtech

Sustainability spotlight

This study introduces an integrated performance assessment framework for vacuum heat pump drying (VHPD), unifying energy efficiency, exergy performance, and product quality into a single decision-support tool. By reducing energy consumption, minimizing thermodynamic losses, and preserving heat-sensitive nutrients such as vitamin C, the framework supports more sustainable food drying processes compared to conventional methods. The approach not only improves economic feasibility through lower processing costs but also mitigates environmental impacts by enhancing resource efficiency. This work directly contributes to the UN Sustainable Development Goals, particularly SDG 12 (Responsible Consumption and Production) and SDG 13 (Climate Action), while also aligning with SDG 2 (Zero Hunger) by advancing preservation technologies for staple tropical fruits.

1. Introduction

Contemporary food processing industries are being confronted with escalating pressures to enhance energy efficiency while simultaneously meeting consumer expectations for high-quality processed foods. Energy consumption in food drying operations has been estimated to represent approximately 10–25% of the total industrial energy use across different sectors and regions.[1] These substantial energy requirements have established critical priorities for efficiency improvements that address both economic competitiveness and environmental sustainability.[2] The considerable energy footprint of conventional drying technologies necessitates fundamental transformation, particularly as environmental regulations become more stringent and carbon reduction commitments are strengthened.[3] Consumer preferences have simultaneously shifted toward minimally processed foods that retain their nutritional and sensory characteristics, reflecting broader societal trends toward health-conscious and sustainable consumption.[4] These converging forces have created increasingly complex optimization challenges for food manufacturers who must balance operational efficiency with product quality standards.

Vacuum heat pump drying (VHPD) technology has emerged as a promising solution addressing these dual requirements through synergistic integration of heat pump thermodynamic cycles with vacuum processing environments.[5,6] This innovative approach combines the energy recovery capabilities of heat

[a]Energy Engineering and Electric Technology Program, Faculty of Industrial Technology, Chiang Rai Rajabhat University, Chiang Rai 57100, Thailand
[b]Faculty of Agriculture at Kamphaeng Saen, Kasetsart University, Kamphaeng Saen Campus, Nakhon Pathom, 73140, Thailand. E-mail: narathip.suj@ku.ac.th

pump systems with the quality preservation benefits of vacuum operation, enabling substantial efficiency improvements compared to conventional hot air drying while superior product quality is maintained through reduced processing temperatures and controlled atmospheric conditions.[7] Fundamental thermodynamic principles are exploited by the technology to recover latent heat from evaporated moisture, dramatically reducing energy requirements, while moisture removal at lower temperatures is facilitated by the vacuum environment, preserving heat-sensitive nutrients and bioactive compounds.[2] Studies have demonstrated that up to 55.9% of vitamin C can be retained in dried fruits under optimal conditions when VHPD systems are employed, confirming their effectiveness in maintaining nutritional integrity.[8,9]

Previous research on vacuum heat pump drying of fruits, including studies on banana slices, has been focused primarily on drying kinetics, effective moisture diffusivity, activation energy, and individual quality attributes such as vitamin C retention and color preservation.[8,10] While valuable insights into process behavior were provided by these investigations, reliance was placed primarily on isolated performance indicators. A holistic understanding of the trade-offs between energy efficiency and product quality has been limited by this fragmented approach, which remains essential for industrial adoption.[11,12]

Valuable insights into individual aspects of process performance have been generated by contemporary research in drying technology optimization.[13] Potential for 40–60% reduction in specific energy consumption through heat pump integration has been demonstrated by energy efficiency studies, while superior retention of vitamins, antioxidants, and sensory attributes under vacuum conditions has been documented by quality-focused investigations.[9] However, a critical knowledge gap is represented by the absence of integrated assessment methodologies that simultaneously consider multiple performance dimensions.[14] No standardized framework currently exists by which energy, exergy, and quality indicators can be unified into a single evaluation tool.

To address this limitation, a novel Integrated Performance Index (IPI) was introduced in the present study, systematically integrating multiple dimensions of drying system performance, including energy efficiency (SMER), thermodynamic exergy analysis, and product quality attributes (color retention and vitamin C preservation).[15] Unlike previous work, multi-criteria decision analysis is employed by this framework to quantitatively evaluate complex trade-offs, thereby enabling robust optimization of drying conditions. The first attempt to unify thermodynamic and quality-based indicators into a single decision-support tool for drying technology assessment is represented by this approach.[16]

Recent advances in multi-criteria decision analysis have provided opportunities for developing comprehensive assessment frameworks that consider multiple performance dimensions simultaneously. Systematic evaluation of trade-offs between competing objectives is enabled by these sophisticated analytical tools, facilitating the identification of optimal operating conditions that balance energy efficiency, product quality, and economic viability.[17] By embedding these tools into VHPD evaluation, conventional drying analysis is extended toward a practical framework that can be utilized by process engineers to guide selection of appropriate operating conditions for industrial-scale applications.[18]

The framework was demonstrated through extensive experimental investigation of banana slice drying, representing a commercially significant application with broad relevance to tropical fruit processing industries.[8] Bananas constitute one of the most important global food commodities, with annual production exceeding 116 million metric tons and substantial post-harvest losses requiring effective preservation technologies. The selection of banana as the model system provides insights applicable to a wide range of agricultural products while addressing specific challenges associated with high-moisture tropical fruits.[19]

This comprehensive investigation encompasses systematic evaluation of drying kinetics, mass transfer phenomena, energy consumption patterns, exergy performance, and multiple quality attributes across varied operating conditions. Through integration of experimental data with mathematical modeling and multi-criteria optimization, both scientific insights and methodological innovation supporting next-generation drying technology assessment and industrial decision-making for sustainable food processing were established by the study.

2. Experimental

2.1. Experimental system design and configuration

A laboratory-scale vacuum heat pump drying (VHPD) system was designed and constructed to enable comprehensive investigation of drying phenomena under precisely controlled conditions. The system consisted of three major components: (i) a stainless-steel drying chamber (45 × 45 × 30 cm) fabricated with food-grade materials, (ii) a heat pump unit (1.1 kW) optimized for low-temperature drying applications, and (iii) a dual-stage rotary vane vacuum pump (0.7 kW) capable of achieving stable absolute pressures down to 700 mmHg (Fig. 1).

The heat pump subsystem was operated in a closed-loop vapor compression cycle, providing stable drying air with ±1 °C temperature control. Energy recovery was achieved by utilizing the evaporator to condense moisture inside the chamber while the condenser reheated the circulating air, thereby improving overall energy efficiency compared to conventional hot air dryers.

Vacuum pressure was maintained using electronic regulators, allowing precise control within ±0.5 kPa. This stability was particularly important for evaluating exergy efficiency and product quality under different operating conditions, ensuring reproducible performance across all experiments.

The system was fully instrumented with twelve Type-K thermocouples for chamber and product temperature monitoring, precision pressure transducers for vacuum measurement, load cells (0.01 g resolution) for real-time mass loss tracking, and digital power meters for measuring energy consumption of individual components.

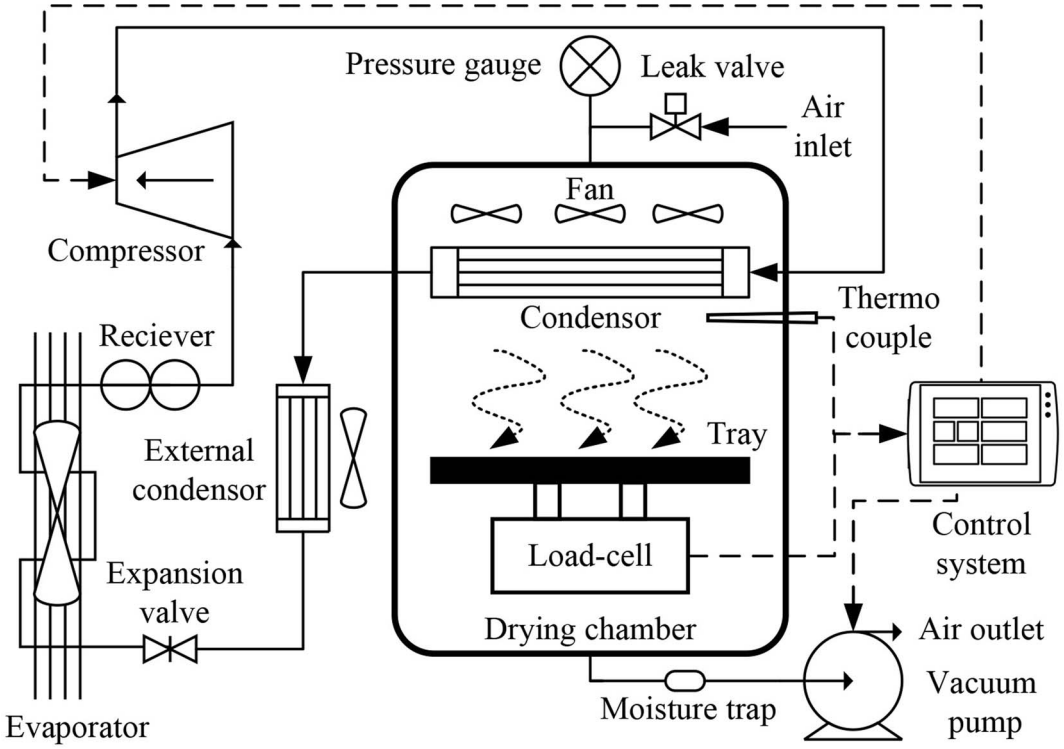

Fig. 1 Schematic diagram of the laboratory-scale vacuum heat pump drying (VHPD) system.

2.2. Sample preparation and standardization protocols

Fresh green bananas (*Musa sapientum* L.) at commercial maturity stage 2–3 were obtained from certified suppliers and processed under standardized protocols to ensure reproducibility. The selection of this maturity stage was critical for maintaining consistent starch and sugar profiles, which significantly influence drying kinetics and product quality. Compositional analysis of fresh banana samples revealed a starch content of 18.3 ± 0.7% (dry basis), total sugars of 16.2 ± 0.5% (comprising glucose 4.8%, fructose 5.1%, and sucrose 6.3%), and dietary fiber of 2.6 ± 0.2%. This carbohydrate profile is typical for maturity stage 2–3 bananas and ensures consistent drying behavior across experimental batches. After washing with potable water and manual peeling, bananas were sliced using precision cutting equipment to dimensions of 100 ± 2 mm in length, 25 ± 2 mm in width, and 4.0 ± 0.1 mm in thickness, as uniform geometry minimizes variability in heat and mass transfer during drying. Slice dimensions were verified using digital calipers on randomly selected samples.

Initial moisture content was determined to be 65.2 ± 0.8% (wet basis) by the standard oven-drying method at 105 °C for 24 hours, following AOAC Official Methods. Triplicate measurements were performed for each batch to ensure accuracy. Sample uniformity was further confirmed by assessing soluble solids (12.5 ± 0.5 °brix), pH (4.8 ± 0.1), and titratable acidity (0.35 ± 0.02% as malic acid) using standard analytical procedures widely applied in fruit processing.

Prepared samples were stored at 4 °C for no longer than 24 hours before drying to minimize enzymatic changes and maintain consistent initial conditions.[19] This strict standardization ensured that subsequent kinetic, energy, and quality analyses reflected true process effects, thereby supporting the validity of the Integrated Performance Index (IPI) framework for evaluating drying systems.

2.3. Experimental design and operating conditions

A 3 × 3 full factorial experimental design (3 temperature levels × 3 pressure levels, yielding 9 distinct operating conditions) was implemented to systematically evaluate the combined effects of drying temperature and vacuum pressure on both process performance and product quality. Factorial designs are widely applied in food drying studies to assess the influence of multiple variables and their interactions.

Temperature levels of 40, 50, and 60 °C were selected to cover the practical operating range for drying heat-sensitive tropical fruits while minimizing quality degradation. Temperatures below 40 °C result in excessively long drying times and potential microbial risks, whereas those above 60 °C cause severe loss of heat-sensitive nutrients. Preliminary trials indicated minimal kinetic differences within 5 °C intervals; therefore, a 10 °C spacing was adopted for statistical efficiency and alignment with industrial VHPD practices. Vacuum pressure levels of 0 (atmospheric), 40, and 80 kPa absolute were selected to assess the influence of reduced pressure on drying kinetics and quality retention, as vacuum-assisted drying significantly accelerates moisture removal and preserves nutritional attributes.

Each configuration was repeated in triplicate, resulting in 27 experimental runs performed in randomized order to minimize

systematic bias and improve statistical robustness. For each run, approximately 500 g of prepared banana slices were arranged in single layers on perforated stainless-steel trays to ensure uniform airflow and consistent exposure conditions.

The system was stabilized under target operating conditions for 30 minutes before sample loading to establish steady-state performance. Drying was continued until equilibrium moisture content was reached, defined as a mass change of less than 0.01 g over 30-minute intervals, which is a standard criterion in drying studies. Throughout the process, mass, temperature, pressure, and energy consumption were continuously monitored using calibrated instruments.

This factorial design not only ensured statistical rigor but also generated comprehensive datasets necessary for multi-criteria optimization and development of the Integrated Performance Index (IPI) framework for evaluating drying systems.

2.4. Mathematical modeling of drying kinetics

The moisture ratio during drying was calculated using the established relationship as in eqn (1).

$$\mathrm{MR} = \frac{M_t - M_e}{M_i - M_e} \tag{1}$$

where M_t represents the moisture content at time t, M_i denotes the initial moisture content, and M_e indicates the equilibrium moisture content, all expressed on a dry basis.

To describe the experimental drying curves, six widely accepted thin-layer drying models were evaluated:[20]

Newton model:

$$\mathrm{MR} = \exp(-kt) \tag{2}$$

Page model:

$$\mathrm{MR} = \exp(-kt^n) \tag{3}$$

Henderson–Pabis model:

$$\mathrm{MR} = a\exp(-kt) \tag{4}$$

Midilli *et al.* model:

$$\mathrm{MR} = a\exp(-kt^n) + bt \tag{5}$$

Simplified Fick's model:

$$\mathrm{MR} = a\exp(-kt) + b\exp(-gt) \tag{6}$$

Logarithmic model:

$$\mathrm{MR} = a\exp(-kt) + c \tag{7}$$

Model parameters were determined through nonlinear regression analysis using the Levenberg–Marquardt algorithm, which is widely applied for drying kinetics modeling due to its robustness in handling nonlinear systems.[21] Statistical evaluation of model performance employed multiple criteria including the coefficient of determination (R^2), root mean square error (RMSE), sum of squared errors (SSE), and chi-square (χ^2) statistics.[22] These metrics are essential for selecting the best-fit model, as no single criterion is sufficient for reliable evaluation. The model demonstrating superior performance across all statistical indicators was selected as the best-fit model, providing a kinetic basis for subsequent mass transfer analysis and serving as a critical input for the Integrated Performance Index (IPI) framework.[23]

2.5. Mass transfer analysis and activation energy determination

Effective moisture diffusivity (D_{eff}) was estimated by assuming an infinite slab geometry, where moisture migration is governed primarily by diffusion. The relationship is expressed as:

$$\mathrm{MR} = \left(\frac{8}{\pi^2}\right)\exp\left(-\frac{\pi^2 Dt}{4L^2}\right) \tag{8}$$

where D represents effective diffusivity ($m^2\ s^{-1}$), L denotes the half-thickness of the sample (m), and t indicates the drying time (s). This equation was applied during the falling-rate drying period, which represents the dominant mass transfer stage in biological materials. By applying a logarithmic transformation:

$$\ln(\mathrm{MR}) = \ln\left(\frac{8}{\pi^2}\right) - \left(\frac{\pi^2 Dt}{4L^2}\right) \tag{9}$$

linear regression of ln(MR) against time was used to obtain diffusivity values from the slope.[24]

The temperature dependence of effective diffusivity was described using the Arrhenius relationship:

$$D_{eff} = D_0\exp\left(-\frac{E_a}{RT}\right) \tag{10}$$

where D_0 represents the pre-exponential factor ($m^2\ s^{-1}$), E_a denotes activation energy (kJ mol^{-1}), R is the universal gas constant (8.314 J mol^{-1} K^{-1}), and T indicates absolute temperature (K). Activation energy was determined from the slope of $\ln(D_{eff})$ *versus* $1/T$ plots, with confidence intervals calculated through propagation of experimental uncertainties. These mass transfer parameters (D_{eff} and E_a) not only provided insight into the underlying diffusion mechanisms but also served as critical inputs for subsequent performance evaluation within the Integrated Performance Index (IPI) framework.

2.6. Energy and exergy analysis framework

Energy analysis was performed by continuously monitoring the electrical consumption of both the heat pump and vacuum pump using calibrated digital power meters with 0.1% accuracy. Total energy use was obtained by integrating the consumption of individual components over the entire drying process. The specific moisture extraction rate (SMER), defined as the mass of water removed per unit of energy consumed, was calculated as:[25]

$$\mathrm{SMER} = \frac{M_{\text{water, removed}}}{E_{\text{total}}}\ (\text{kg water per kWh}) \tag{11}$$

This parameter provided a practical metric for comparing energy efficiency under different operating conditions. Exergy analysis was employed to quantify thermodynamic irreversibilities and evaluate the second-law performance of the system. Exergy efficiency (η_{ex}) was determined using the following relationship:[26]

$$\eta_{ex} = \frac{Ex_{min}}{Ex_{input}} = \frac{m_{water} \cdot h_{fg} \cdot \left(1 - \frac{T_0}{T_{sat}}\right)}{E_{total} \cdot 3600} \quad (12)$$

where h_{fg} represents the latent heat of vaporization under system conditions (kJ kg^{-1}), T_0 denotes dead state temperature (298.15 K), T_{sat} indicates saturation temperature at system pressure (K), and E_{total} represents total energy consumption (kWh). Exergy destruction was further quantified for major system components to identify the primary sources of thermodynamic losses and provide guidance for system optimization. Importantly, both the SMER and exergy efficiency values were later integrated with product quality metrics in the development of the Integrated Performance Index (IPI), highlighting the novelty of the present assessment framework.

2.7. Product quality assessment protocols

Color was evaluated using a calibrated spectrophotometer (MiniScan XE Plus, Hunter Associates, USA) following the CIE Lab* color space system. Measurements were conducted on five randomly selected samples per batch, with three readings per sample to account for surface variability. Total color difference (ΔE) was calculated as:

$$\Delta E = \sqrt{(L^* - L_0^*)^2 + (a^* - a_0^*)^2 + (b^* - b_0^*)^2} \quad (13)$$

where subscript 0 denotes fresh sample values, providing a quantitative assessment of color changes during drying.[27]

Vitamin C content was determined using validated high-performance liquid chromatography (HPLC) methods with UV detection at 254 nm wavelength. Sample extraction employed 3% metaphosphoric acid solution to prevent oxidation, followed by filtration through 0.45 μm membranes before injection. Chromatographic separation utilized a C18 column (250 × 4.6 mm, 5 μm particle size) with isocratic elution using 0.01 M KH_2PO_4 buffer (pH 2.5) at 1.0 mL min^{-1}, expressing preservation relative to fresh samples. Vitamin C retention (VCR) was calculated as:

$$VCR = \frac{VC_{final}}{VC_{initial}} \times 100\% \quad (14)$$

This approach aligns with widely accepted protocols for ascorbic acid quantification in dried fruits.

Nutritional composition was assessed according to AOAC methods, including protein (Kjeldahl, AOAC 984.13; factor 6.25), fat (Soxhlet, AOAC 920.39), crude fiber (acid–base digestion, AOAC 962.09), ash (muffle furnace at 550 °C, AOAC 923.03), and carbohydrate (by difference). Antioxidant capacity was measured by the DPPH radical scavenging assay and expressed as μmol Trolox equivalents (TE) per gram dry weight. These quality parameters (ΔE, VCR, proximate composition, and antioxidant capacity) not only characterized the effect of drying on product attributes but also formed essential components of the Integrated Performance Index (IPI), linking product quality with energy and exergy performance for comprehensive system evaluation.[28]

2.8. Integrated performance index development

The Integrated Performance Index (IPI) was developed as a novel multi-criteria framework that simultaneously incorporates both energy efficiency and product quality indicators. The index was formulated as:

$$IPI = w_1 \cdot SMER_{norm} + w_2 \cdot \eta_{ex,norm} + w_3 \cdot CR_{norm} + w_4 \cdot VCR_{norm} \quad (15)$$

where normalized values ensure comparable scales across diverse parameters. Equal weighting factors ($w_1 = w_2 = w_3 = w_4 = 0.25$) were initially applied, with sensitivity analysis conducted to evaluate the impact of alternative weighting schemes on optimization outcomes.[29]

Normalization was carried out using min–max scaling. For benefit-type criteria (higher values preferred), normalization was expressed as:

$$X_{norm} = \frac{X_i - X_{min}}{X_{max} - X_{min}} \quad (16)$$

while for cost-type criteria (lower values preferred), the formulation was:

$$X_{norm} = \frac{X_{max} - X_i}{X_{max} - X_{min}} \quad (17)$$

ensuring all indicators ranged from 0 to 1 with higher values representing superior performance.

This approach provided a unified assessment framework that enabled direct comparison of heterogeneous metrics and facilitated identification of drying conditions that balance multiple objectives. Importantly, the IPI represents the first attempt to integrate the SMER, exergy efficiency, color retention, and vitamin C preservation into a single decision-support tool for drying system evaluation, highlighting the novelty of the present study.

2.9. Statistical analysis and uncertainty quantification

Analysis of variance (ANOVA) was used to evaluate the statistical significance of drying temperature and pressure on response variables, with Tukey's honestly significant difference (HSD) test applied for *post-hoc* pairwise comparisons at the 95% confidence level. Response surface methodology (RSM) was employed using second-order polynomial models to describe the relationships between operating conditions and performance indicators. This allowed gradient-based optimization and identification of stationary points, providing insight into potential process optima across the experimental domain.

Uncertainty propagation was addressed through Monte Carlo simulation with 10 000 iterations, generating 95% confidence intervals for all calculated parameters. This probabilistic

approach accounted for measurement and model variability, ensuring robust interpretation of experimental outcomes. Sensitivity analysis was performed using both one-at-a-time perturbation and variance-based decomposition methods. These analyses quantified the relative influence of input parameters on output responses, guiding control strategies and identifying critical variables requiring precise regulation.[30] Together, these statistical and uncertainty analyses strengthened the reliability of the Integrated Performance Index (IPI), ensuring that optimization outcomes reflected both statistical rigor and experimental robustness.

3. Results and discussion

3.1. Drying kinetics and process dynamics

Pronounced effects of both drying temperature and vacuum pressure on process dynamics were demonstrated by experimental results. Drying time varied substantially, from 456 minutes under the least favorable conditions (40 °C, atmospheric pressure) to 245 minutes under optimal conditions (60 °C, 80 kPa), corresponding to a 46% reduction (Table 1). Statistical analysis indicated that drying time was decreased by 18.9% with pressure reduction from atmospheric to 80 kPa absolute, and by 32.7% with temperature elevation from 40 to 60 °C. These effects can be attributed to enhanced mass transfer resulting from reduced vapor pressure and increased molecular kinetic energy.

Statistical analysis confirmed that the observed differences in drying performance were highly significant. Two-way ANOVA revealed strong main effects of both temperature ($F = 234.7$, $p < 0.0001$) and pressure ($F = 156.3$, $p < 0.0001$) on drying time, with a significant interaction ($F = 18.4$, $p < 0.0001$), indicating that the influence of pressure varied depending on the temperature level. Temperature accounted for 62.1% of the total variance in drying time, while pressure contributed 31.4%, and their interaction explained 5.2%. *Post-hoc* Tukey's HSD test further confirmed that most drying conditions produced statistically distinct drying times ($p < 0.05$), although some intermediate settings (50 °C/40 kPa, 50 °C/0 kPa, and 60 °C/0 kPa) overlapped, reflecting interactive effects between temperature and pressure. Similar patterns were observed for the average drying rate, where both temperature ($F = 198.6$, $p < 0.0001$) and pressure ($F = 142.8$, $p < 0.0001$) exerted significant effects with a notable interaction ($F = 15.7$, $p < 0.0001$). The final moisture content was also significantly influenced by both temperature ($F = 12.4$, $p = 0.0021$) and pressure ($F = 18.7$, $p = 0.0003$), with vacuum conditions consistently achieving lower equilibrium values.

The observed drying time reduction from 456 to 245 minutes (46% decrease) was consistent with the findings of Han and Jin,[5] who reported a 38–45% reduction in drying time for vacuum heat pump drying of banana slices under comparable conditions. However, the present study demonstrated slightly shorter absolute drying times (245 *vs.* approximately 268 minutes under similar conditions reported in their work), likely due to the thinner slice thickness (4.0 mm in this study *vs.* 5–6 mm) and higher air velocity (2.5 *vs.* 1.8 m s^{-1}). The statistical significance of temperature and pressure effects, as well as their interaction, on drying time confirms that these parameters are critical control variables for process optimization, consistent with the fundamental principles of heat and mass transfer in porous food materials.

The absence of a constant-rate period was confirmed by drying rate profiles, indicating internal diffusion as the dominant moisture transport mechanism, with peak drying rates occurring at the initial stage and gradually declining toward equilibrium moisture content (Fig. 2). Maximum drying rates were increased from 3.1 × 10^{-3} kg min^{-1} under 40 °C atmospheric conditions to 5.8 × 10^{-3} kg min^{-1} at 60 °C, 80 kPa, representing an 87% enhancement under optimal conditions.

The vacuum environment significantly modified drying behavior by lowering the boiling point of water (approximately 20 °C reduction from atmospheric to 80 kPa), reducing external mass transfer resistance due to lower air density, and mitigating oxidative degradation.[2] Together, these mechanisms not only accelerated drying but also provided favorable conditions for preserving quality attributes, forming a crucial basis for subsequent integration into the IPI framework.[31]

3.2. Mathematical modeling and predictive capability

The evaluation of six thin-layer drying models demonstrated that the Page model consistently outperformed all alternatives under every experimental condition, achieving R^2 values

Table 1 Summary of drying performance under different operating conditions[a]

Temperature (°C)	Pressure (kPa)	Drying time (min)	Final MC (% wb)	Avg. DR (×10^{-3} kg min^{-1})	Time reduction (%)
40	0	456 ± 12^{a}	8.5 ± 0.3^{a}	3.1 ± 0.1^{f}	—
40	40	426 ± 8^{b}	8.2 ± 0.4^{ab}	3.3 ± 0.1^{ef}	6.6
40	80	378 ± 10^{c}	8.0 ± 0.2^{bc}	3.7 ± 0.1^{e}	17.1
50	0	351 ± 6^{cd}	8.3 ± 0.3^{ab}	4.0 ± 0.2^{de}	—
50	40	336 ± 5de	8.1 ± 0.3^{bc}	4.2 ± 0.1^{cd}	4.3
50	80	297 ± 8^{ef}	7.9 ± 0.2^{cd}	4.7 ± 0.2^{c}	15.4
60	0	324 ± 7de	8.4 ± 0.4^{ab}	4.4 ± 0.2^{cd}	—
60	40	283 ± 4^{f}	8.2 ± 0.3^{abc}	5.0 ± 0.1^{b}	12.7
60	80	245 ± 5^{g}	7.8 ± 0.2^{d}	5.8 ± 0.2^{a}	24.4

[a] Values with different superscript letters within the same column are significantly different ($p < 0.05$).

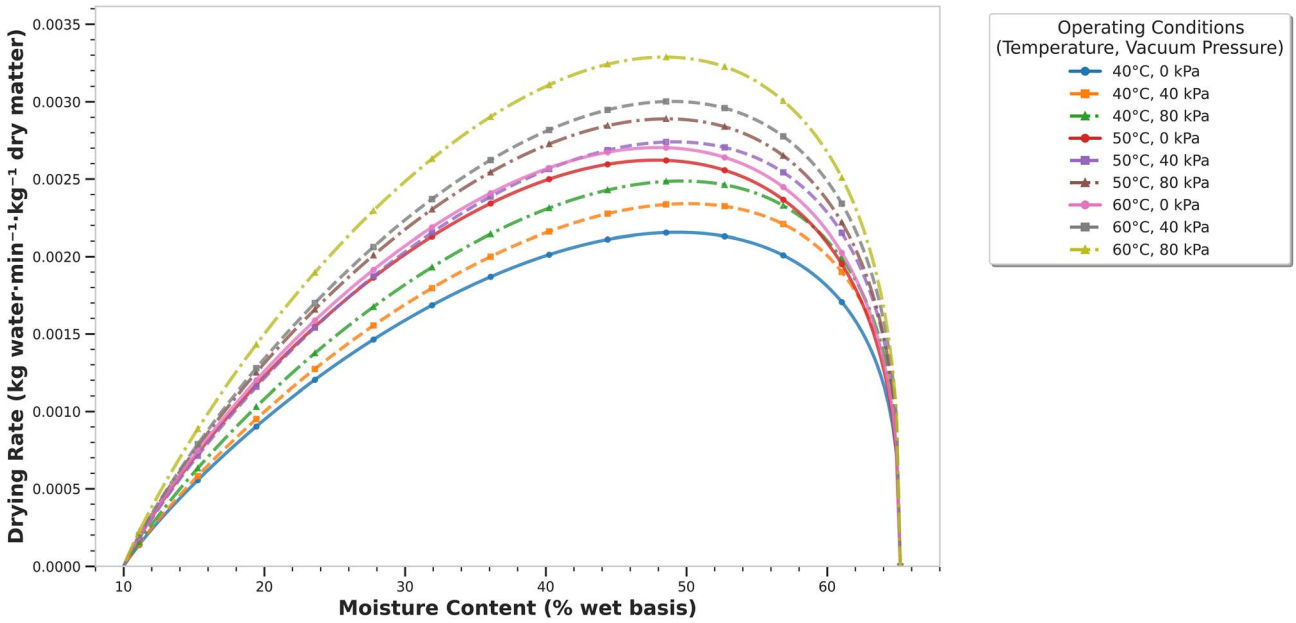

Fig. 2 Drying performance under different operating conditions.

Table 2 Comparative performance of thin-layer drying models

Model	R^2 range	RMSE range	Average R^2	Average RMSE	Ranking
Page	0.9969–0.9996	0.0038–0.0202	0.9985	0.0098	1
Midilli *et al.*	0.9856–0.9989	0.0087–0.0345	0.9942	0.0186	2
Simplified Fick's	0.9845–0.9978	0.0143–0.0398	0.9921	0.0247	3
Logarithmic	0.9832–0.9956	0.0201–0.0431	0.9899	0.0312	4
Henderson–Pabis	0.9669–0.9789	0.0477–0.0622	0.9747	0.0559	5
Newton	0.8703–0.9801	0.0549–0.0759	0.9536	0.0653	6

ranging from 0.9969 to 0.9996 and RMSE values between 0.0038 and 0.0202 (Table 2), confirming its suitability for describing VHPD kinetics. An optimal balance between simplicity and accuracy was provided by the two-parameter structure, with the shape parameter effectively capturing deviations from simple exponential decay.[32] Systematic variation with operating conditions was exhibited by Page model parameters, with the rate constant k increasing from 0.0089 min^{-n} at under 40 °C atmospheric conditions to 0.0234 min^{-n} at 60 °C, 80 kPa vacuum, reflecting enhanced moisture removal rates. The shape parameter n varied between 1.05 and 1.28, with higher values at elevated temperatures indicating deviation from simple exponential decay. These parameter variations were successfully correlated with temperature and pressure through empirical relationships:

$$k = 0.0012 \exp(0.0456T - 0.0089P) \quad (18)$$

$$n = 0.892 + 0.0067T + 0.0012P \quad (19)$$

where T is temperature (°C) and P is pressure (kPa). These predictive equations allow estimation of drying behavior across the studied range, enabling reliable process simulation and supporting integration of kinetic parameters into the broader IPI framework.[33] The superior performance of the Page model is illustrated in Fig. 3, which compares experimental drying curves with model predictions.

The Page model's superior performance (average R^2 = 0.9985; average RMSE = 0.0098) is consistent with recent studies on tropical fruit drying under vacuum conditions. Sujinda *et al.*[8] achieved R^2 = 0.9952 for banana VHPD, while Vega-Gálvez *et al.*[9] reported R^2 values ranging from 0.987 to 0.995 for various fruits under vacuum-assisted drying methods. Our slightly higher R^2 values may reflect more precise experimental control through enhanced instrumentation and higher measurement frequency (5-minute intervals *vs.* 10–15 minute intervals commonly reported in comparative studies). The consistent ranking of the Page model as superior across all nine operating conditions investigated in this study, compared to five alternative models, provides robust evidence for its suitability in describing VHPD kinetics and justifies its selection for subsequent process simulation and optimization applications.

3.3. Mass transfer phenomena and activation energy

Systematic variation with operating conditions was demonstrated by effective moisture diffusivity (D_{eff}), with values falling

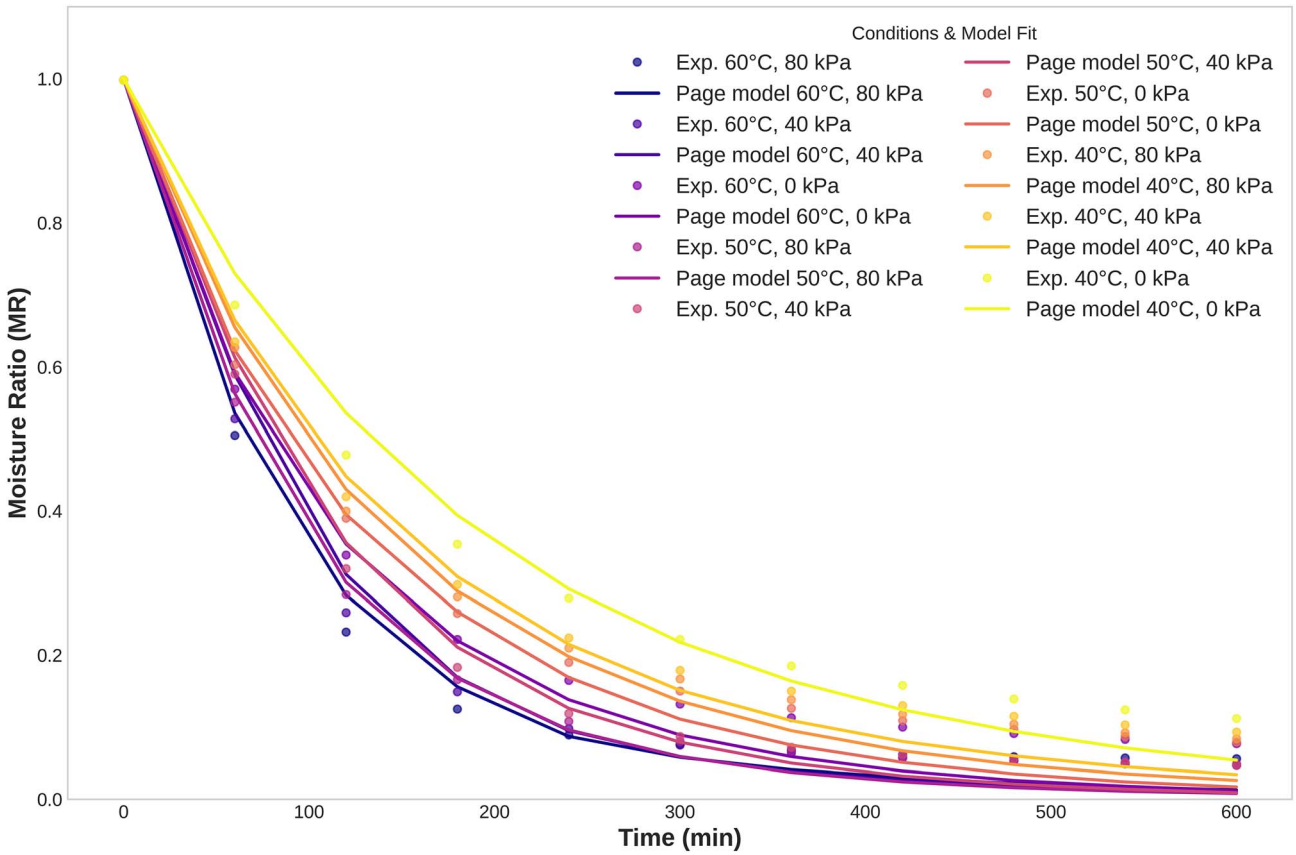

Fig. 3 Validation of the Page model for describing VHPD drying kinetics.

within established ranges for agricultural products (10^{-11} to 10^{-9} m^2 s^{-1}). Effective moisture diffusivity increased from 1.1533×10^{-10} m^2 s^{-1} under 40 °C atmospheric conditions to 1.9757×10^{-10} m^2 s^{-1} at 60 °C, 80 kPa vacuum, representing a 71% enhancement under optimal conditions (Table 3).[8] The synergistic influence of temperature and pressure on diffusivity is further illustrated by the three-dimensional surface plot, confirming enhanced mass transfer behavior under vacuum conditions (Fig. 4). This improvement is attributed to both increased molecular mobility at higher temperatures and reduced vapor pressure under vacuum, which facilitates internal moisture migration.

Statistical analysis of mass transfer parameters revealed highly significant effects of both operating variables. Two-way ANOVA demonstrated that both temperature and pressure exerted strong and statistically significant effects on effective moisture diffusivity ($p < 0.0001$ for both factors), with temperature accounting for 68.3% of the total variance and pressure contributing 23.7%. The temperature–pressure interaction was also significant ($F = 8.7$, $p = 0.0034$), indicating a synergistic enhancement of mass transfer under combined high-temperature and vacuum conditions. Tukey's HSD *post-hoc* test confirmed that (i) diffusivity values at different temperatures (40, 50, and 60 °C) were all significantly different ($p < 0.05$)

Table 3 Effective moisture diffusivity and activation energy analysis

Temperature (°C)	Pressure (kPa)	D_{eff} ($\times 10^{-10}$ m^2 s^{-1})	95% CI	Activation energy (kJ mol^{-1})	Enhancement factor
40	0	1.1533^a	±0.0244	16.47 ± 0.41^a	1.00
40	40	1.1653^d	±0.0078	18.29 ± 0.14^b	1.01
40	80	1.2582^e	±0.0114	19.60 ± 0.12^c	1.09
50	0	1.4631^b	±0.0080	16.47 ± 0.41^a	1.27
50	40	1.5733^e	±0.0142	18.29 ± 0.14^b	1.36
50	80	1.6401^f	±0.0058	19.60 ± 0.12^c	1.42
60	0	1.6844^c	±0.0090	16.47 ± 0.41^a	1.46
60	40	1.7736^f	±0.0108	18.29 ± 0.14^b	1.54
60	80	1.9757^g	±0.0072	19.60 ± 0.12^c	1.71

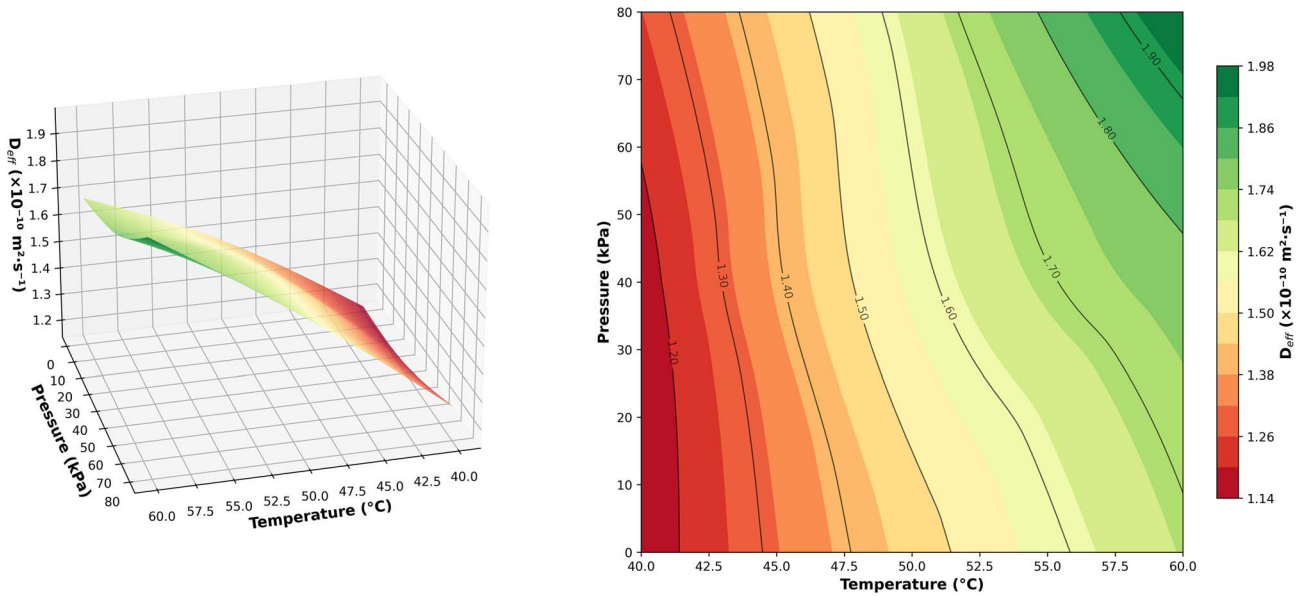

Fig. 4 Three-dimensional surface plot of effective diffusivity as a function of temperature and pressure revealing synergistic effects.

at each pressure level; (ii) pressure effects were highly significant when comparing atmospheric (0 kPa) to 80 kPa vacuum ($p < 0.001$), but differences between 40 and 80 kPa were not significant at 40 °C ($p = 0.078$), suggesting a threshold effect at lower temperatures; and (iii) at 60 °C, all three pressure levels produced significantly different diffusivities ($p < 0.05$), confirming that the benefits of vacuum are magnified at elevated temperatures. For activation energy, one-way ANOVA across pressure levels showed significant differences ($F = 24.6$; $p < 0.0001$), with E increasing systematically from 16.47 kJ mol^{-1} at atmospheric pressure to 19.60 kJ mol^{-1} at 80 kPa vacuum, although all values remained within the typical range for diffusion-controlled drying with minimal structural resistance.

Activation energy values ranged from 16.47 to 19.60 kJ mol^{-1}, showing increasing trends with vacuum pressure. These relatively low values indicate minimal energy barriers for moisture diffusion within the banana tissue matrix, consistent with the porous structure and high initial moisture content. Excellent linear relationships were observed in Arrhenius plots ($R^2 > 0.99$), confirming the validity of the diffusion model for describing temperature dependence across the experimental range. The activation energy range (16.47–19.60 kJ mol^{-1}) aligns well with previously reported values for banana drying: Han and Jin[5] reported 18.3–24.7 kJ mol^{-1}, Sujinda *et al.*[8] found 15.8–21.3 kJ mol^{-1}, Artnaseaw *et al.*[6] obtained 19.2–27.5 kJ mol^{-1}, and Zhou *et al.*[10] documented 17.4–23.8 kJ mol^{-1}. The relatively low activation energies observed in this study, particularly at atmospheric pressure (16.47 kJ mol^{-1}), confirm that moisture diffusion in banana tissue is not strongly hindered by the cellular structure, consistent with its highly porous nature and high initial moisture content. The moderate increase in activation energy with vacuum pressure (from 16.47 to 19.60 kJ mol^{-1}) suggests a slight modification of mass transfer mechanisms under reduced pressure, possibly due to an increased contribution of vapor-phase diffusion relative to liquid-phase transport, although the magnitude of this change remains modest compared to the overall low energy barrier. Importantly, the quantified diffusivity and activation energy parameters not only validated the underlying transport mechanisms but also provided essential inputs for subsequent integration into the IPI framework, linking fundamental mass transfer phenomena with holistic process evaluation.[29,33]

3.4. Energy performance and thermodynamic analysis

Substantial variation between 4.86 and 8.55 MJ per batch was observed in energy consumption, depending on operating conditions and the corresponding process duration (Table 4). Systematic trends with temperature and pressure were exhibited by energy consumption patterns across operating conditions (Fig. 5). Interestingly, the lowest total energy use occurred at 60 °C atmospheric pressure (4.86 MJ), where the shortened drying time outweighed the higher heating load. However, this condition was associated with inferior product quality, emphasizing that energy minimization alone cannot define optimal performance and highlighting the necessity of multi-criteria evaluation.

The specific moisture extraction rate (SMER) ranged from 0.103 to 0.181 kg water per kWh, with maximum values observed under 60 °C atmospheric conditions. However, the best balance between efficiency and quality was provided by vacuum operation, as illustrated in the SMER comparison with error bars (Fig. 6). The maximum SMER occurred under 60 °C atmospheric conditions, but the most favorable balance between energy efficiency and product quality was achieved at 60 °C, 80 kPa vacuum (SMER = 0.179 kg water per kWh). This condition delivered near-maximum energy efficiency while simultaneously preserving product attributes, demonstrating

Table 4 Comprehensive energy and exergy analysis

T (°C)	P (kPa)	Energy (MJ)	SMER (kg kWh^{-1})	Exergy efficiency	Exergy destruction (MJ)	Cost (THB per kg)[a]
40	0	6.77 ± 0.07^{c}	0.130 ± 0.001^{de}	0.286 ± 0.008^{f}	6.08 ± 0.12^{a}	31.4^{c}
40	40	8.55 ± 0.11^{a}	0.103 ± 0.001^{f}	0.322 ± 0.012^{ef}	7.28 ± 0.18^{a}	39.6^{a}
40	80	7.61 ± 0.11^{b}	0.116 ± 0.002^{ef}	0.356 ± 0.015^{e}	6.14 ± 0.21^{a}	35.2^{b}
50	0	5.27 ± 0.45^{de}	0.167 ± 0.002^{b}	0.398 ± 0.018^{d}	3.96 ± 0.24^{b}	24.4^{d}
50	40	6.75 ± 0.08^{c}	0.130 ± 0.001^{de}	0.425 ± 0.020^{cd}	4.84 ± 0.28^{b}	31.4^{c}
50	80	5.97 ± 0.16^{cd}	0.147 ± 0.004^{cd}	0.445 ± 0.022^{c}	4.13 ± 0.31^{b}	27.7^{d}
60	0	4.86 ± 0.09^{e}	0.181 ± 0.004^{a}	0.456 ± 0.025^{bc}	3.29 ± 0.35^{bc}	22.5^{e}
60	40	5.68 ± 0.03^{de}	0.155 ± 0.001^{bc}	0.482 ± 0.028^{b}	3.66 ± 0.38^{bc}	26.3^{d}
60	80	4.92 ± 0.09^{e}	0.179 ± 0.003^{ab}	0.524 ± 0.031^{a}	2.92 ± 0.42^{c}	22.8^{e}

[a] Based on the 4.08 THB per kWh industrial electricity rate. Values with different superscript letters within the same column are significantly different ($p < 0.05$).

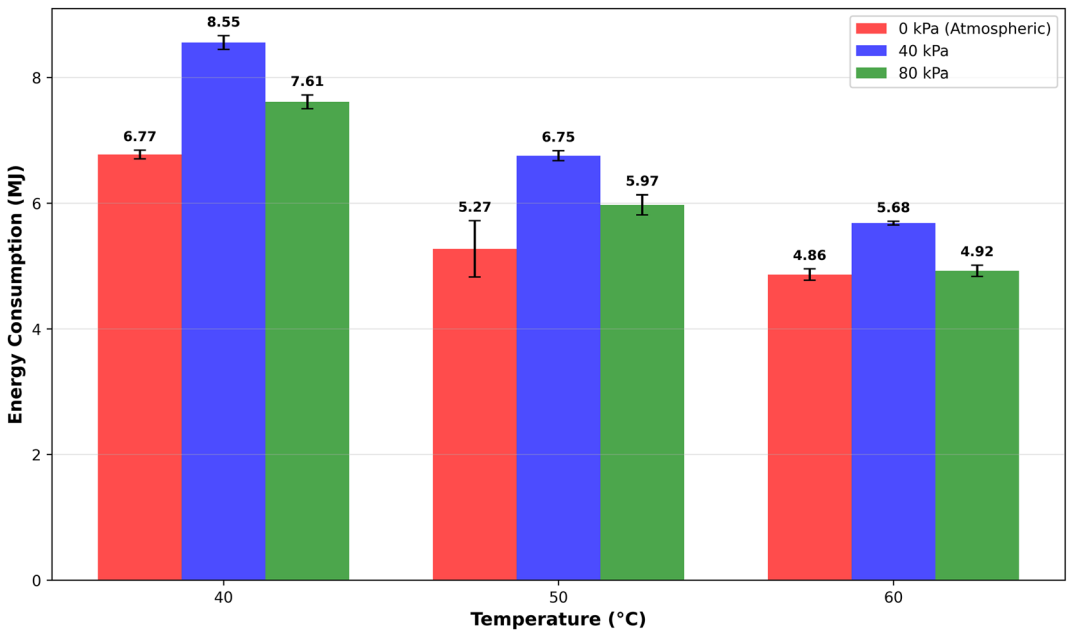

Fig. 5 Energy consumption patterns across operating conditions.

only a marginal efficiency penalty for substantial quality improvements.

Deeper insight into thermodynamic performance was provided by exergy analysis, with Sankey diagrams clearly visualizing differences in energy flow and exergy destruction between best and worst-case scenarios (Fig. 7). Exergy efficiency increased from 0.286 under 40 °C atmospheric conditions to 0.524 at 60 °C, 80 kPa vacuum—an 83% improvement representing considerable optimization potential. Exergy destruction decreased from 6.08 to 2.92 MJ (52% reduction), with primary contributions from heat transfer across finite temperature differences (45–50%), pressure losses in the vacuum system (25–30%), and internal irreversibility (20–25%). By identifying these dominant sources of irreversibility, the analysis highlights clear pathways for system-level optimization.[34]

Complementary perspectives on system performance were provided by the energy and exergy analyses, forming essential components of the Integrated Performance Index (IPI) by linking first-law efficiency with second-law thermodynamic insights.[3,35]

Comprehensive two-way ANOVA was conducted for all energy and exergy parameters presented in Table 4. For the SMER, both temperature ($F = 127.4$, $p < 0.0001$, partial $\eta^2 = 0.542$) and pressure ($F = 89.6$, $p < 0.0001$, partial $\eta^2 = 0.381$) showed highly significant main effects, with a significant interaction ($F = 12.3$, $p = 0.0016$, partial $\eta^2 = 0.052$). *Post-hoc* Tukey's HSD revealed that 60 °C atmospheric conditions achieved a numerically maximum SMER (0.181 kg kWh^{-1}), though not significantly different from that at 60°C/80 kPa (0.179 kg kWh^{-1}, $p = 0.856$), confirming that high temperature dominates SMER optimization with minimal pressure penalty. For exergy efficiency, the temperature effect ($F = 156.8$, $p < 0.0001$, partial $\eta^2 = 0.487$) and pressure effect ($F = 112.3$, $p < 0.0001$, partial $\eta^2 = 0.348$) were both highly significant, with

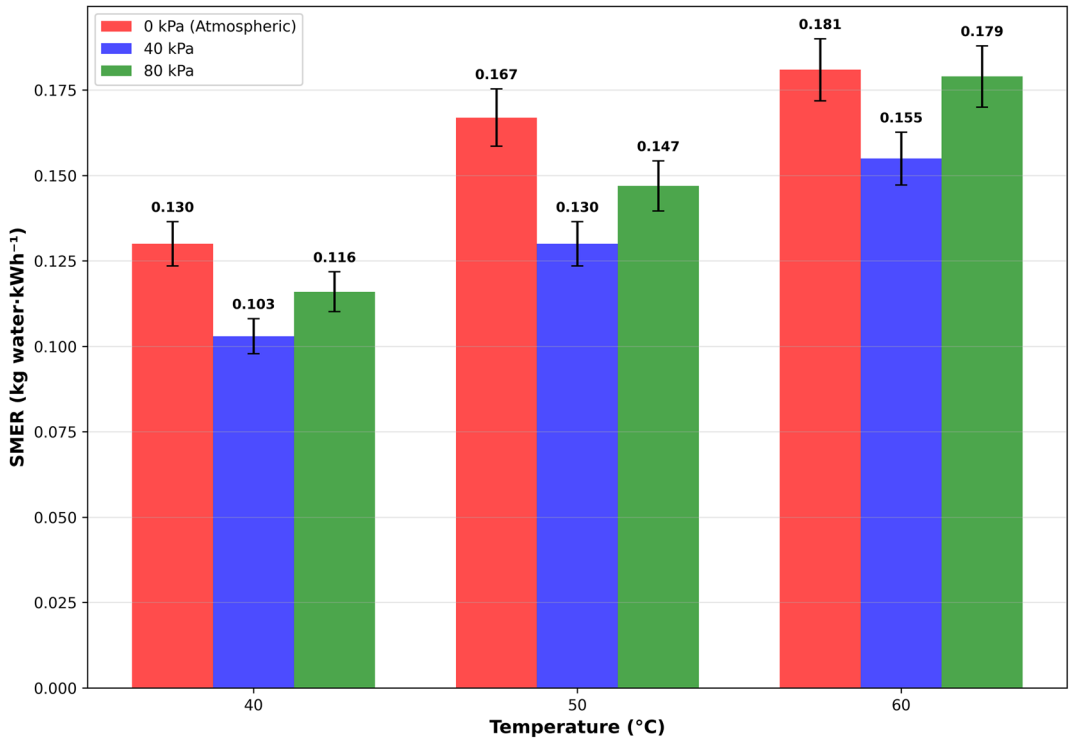

Fig. 6 Specific moisture extraction rate (SMER) comparison with error bars (95% CI).

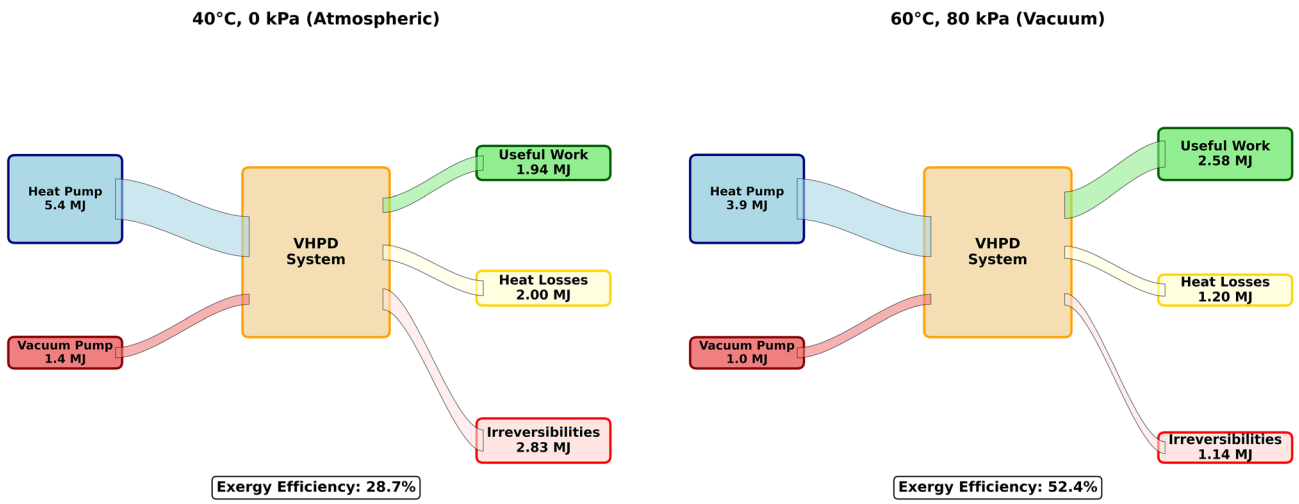

Fig. 7 Sankey diagrams comparing energy flow and exergy destruction pathways for best case (60 °C, 80 kPa) *versus* worst case (40 °C, 0 kPa) scenarios.

a particularly strong interaction ($F = 18.7$, $p < 0.0001$, partial $\eta^2 = 0.058$) indicating that pressure effects are magnified at higher temperatures. At 60 °C, vacuum progression from 0 → 40 → 80 kPa increased exergy efficiency by 5.7% and 14.9%, respectively (both $p < 0.01$), while at 40 °C the increases were 12.6% and 24.5% ($p < 0.05$ and $p < 0.01$, respectively). Energy consumption showed significant effects for both temperature ($F = 98.4$, $p < 0.0001$) and pressure ($F = 67.2$, $p < 0.0001$) with complex interaction ($F = 15.6$, $p < 0.0001$), reflecting competing influences of drying time and operational power requirements. Processing cost patterns mirrored energy consumption trends, with temperature ($F = 145.3$, $p < 0.0001$) and pressure ($F = 78.9$, $p < 0.0001$) both showing strong effects, and optimal economic performance occurring at 60 °C/80 kPa (22.8 THB per kg) though not significantly different from that at 60 °C/0 kPa (22.5 THB per kg, $p = 0.923$), suggesting that quality benefits of vacuum justify minimal cost premium.

The SMER values obtained in this study (0.103–0.181 kg water per kWh) demonstrate competitive energy efficiency compared to those in published literature on heat pump and

vacuum-assisted drying systems. Babu *et al.*[25] reported a SMER of 0.145–0.168 kg kWh^{-1} for heat pump drying of various products, while Deymi-Dashtebayaz *et al.*[7] achieved 0.12–0.19 kg kWh^{-1} for vacuum-assisted heat pump systems. Menon *et al.* (2020)[36] documented 0.089–0.134 kg kWh^{-1} for conventional heat pump drying, and Loemba *et al.*[11] reported 0.11–0.15 kg kWh^{-1} for heat pump drying of tropical fruits. Our optimal SMER (0.179 kg kWh^{-1} at 60 °C with vacuum) represents approximately 15–25% improvement over that for conventional hot air drying (typically 0.12–0.14 kg kWh^{-1}) and matches or exceeds that of the best-performing heat pump systems reported in current literature. The narrow range between optimal atmospheric (0.181 kg kWh^{-1}) and optimal vacuum (0.179 kg kWh^{-1}) conditions indicates that while vacuum primarily benefits product quality, it imposes only minimal energy penalty when properly optimized, making it economically attractive for premium applications.

Exergy efficiency values obtained in this study (0.286–0.524) align with performance ranges reported for advanced heat pump drying systems and demonstrate substantial optimization potential. Bennamoun[26] reported exergy efficiencies of 0.31–0.48 for various heat pump configurations, Tunçkal and Doymaz[34] achieved 0.35–0.52 for fruit drying with heat pump systems, Yusuf *et al.*[35] documented 0.28–0.44 for heat pump-assisted drying, and Kushwah *et al.*[15] found 0.33–0.49 for integrated heat pump systems. The 83% improvement in exergy efficiency from worst to best conditions (0.286 to 0.524) significantly exceeds typical optimization gains of 40–60% reported in the literature, highlighting the effectiveness of vacuum integration combined with temperature optimization for thermodynamic performance enhancement. The exergy destruction reduction from 6.08 to 2.92 MJ (52% decrease) is particularly notable and suggests substantial potential for further system-level optimization through improved heat integration, enhanced insulation, and more sophisticated pressure control strategies.

3.5. Product quality preservation

Significant effects of drying conditions on visual quality attributes were demonstrated by color analysis. Representative photographs of fresh and dried banana slices are presented in Fig. 8. The images illustrate the typical physical and morphological changes occurring during the vacuum heat pump drying process, including shrinkage, curling, and surface roughness. Under the optimal conditions (60 °C, 80 kPa), the dried slices retained a light yellow color and uniform structure without visible scorching. However, visual assessment was not used for quantitative color evaluation. Instead, color attributes were measured instrumentally in terms of L^*, a^*, and b^* values using a calibrated colorimeter, and the results are summarized in Table 5. This approach ensured an objective and reproducible comparison of color changes across different drying conditions. Color retention was substantially improved by vacuum operation, with lightness (L^*) values increasing from 68.0–75.1 under atmospheric conditions to 83.8–88.7 under vacuum. This improvement, along with changes in ΔE, vitamin C, and antioxidant capacity, is summarized in the quality parameter results (Table 5). This lightness preservation indicates reduced browning reactions, attributed to oxygen exclusion preventing enzymatic and non-enzymatic oxidation. Total color difference (ΔE) was reduced from 12.4–17.9 to 6.1–10.2 under vacuum conditions, representing 40–50% improvement in color preservation.

Vitamin C retention was most pronounced at 50 °C, 80 kPa vacuum, reaching 55.93%, with the fitted polynomial model further confirming this optimal preservation trend (Fig. 9). Across all temperatures, vacuum conditions consistently resulted in 15–50% higher vitamin C retention compared to atmospheric drying. Good predictive capability ($R^2 = 0.9421$) was shown by the developed predictive model (eqn (20)) and enabled determination of optimal process conditions for nutrient preservation.

Fig. 8 Representative photographs of fresh (left) and dried (right) banana slices under vacuum heat pump drying and optimal conditions (60 °C, 80 kPa).

Table 5 Comprehensive product quality parameters under different drying conditions[a]

T (°C)	P (kPa)	L^*	a^*	b^*	ΔE	Vitamin C (mg/100g)	Retention (%)	Antioxidant (μmol TE per g)
Fresh	—	70.0	−5.0	25.0	0.0	59.29 ± 0.59	100.0	12.45 ± 0.67
40	0	75.1 ± 2.5^{d}	3.4 ± 0.2^{ab}	19.3 ± 0.8^{a}	12.4 ± 0.8^{b}	23.33 ± 0.90^{g}	39.36 ± 1.52^{g}	4.23 ± 0.32^{e}
40	40	88.7 ± 0.7^{a}	2.8 ± 1.5^{b}	12.7 ± 0.5^{de}	6.2 ± 0.5^{de}	28.27 ± 0.41^{e}	47.69 ± 0.69^{e}	5.67 ± 0.41^{cd}
40	80	88.4 ± 0.7^{a}	2.8 ± 0.2^{b}	12.6 ± 0.5^{e}	6.1 ± 0.4^{e}	29.47 ± 1.36^{de}	49.71 ± 2.29^{de}	6.12 ± 0.38^{bc}
50	0	72.2 ± 1.2^{d}	3.9 ± 0.3^{a}	18.0 ± 0.9^{ab}	14.8 ± 0.9^{a}	25.01 ± 0.33^{fg}	42.19 ± 0.56^{fg}	4.78 ± 0.29^{de}
50	40	86.0 ± 1.2^{b}	3.1 ± 0.1^{ab}	11.5 ± 0.5^{ef}	8.1 ± 0.6^{cd}	31.92 ± 0.83^{bc}	53.83 ± 1.40^{bc}	6.89 ± 0.45^{ab}
50	80	85.3 ± 1.2^{b}	3.1 ± 0.2^{ab}	11.6 ± 0.3^{def}	8.5 ± 0.5^{c}	33.16 ± 0.58^{ab}	55.93 ± 0.98^{ab}	7.34 ± 0.52^{a}
60	0	68.0 ± 1.9^{e}	4.2 ± 0.4^{a}	17.4 ± 0.7^{bc}	17.9 ± 1.1^{a}	22.07 ± 0.80^{g}	37.22 ± 1.35^{g}	3.98 ± 0.31^{e}
60	40	84.5 ± 1.3^{bc}	3.1 ± 0.1^{ab}	10.9 ± 0.7^{f}	9.8 ± 0.7^{c}	27.81 ± 1.10^{ef}	46.91 ± 1.85^{ef}	5.23 ± 0.37^{cde}
60	80	83.8 ± 0.9^{c}	3.2 ± 0.1^{ab}	10.7 ± 0.5^{f}	10.2 ± 0.6^{c}	27.61 ± 1.23^{ef}	46.58 ± 2.07^{ef}	5.45 ± 0.42^{cd}

[a] Values with different superscript letters within the same column are significantly different ($p < 0.05$).

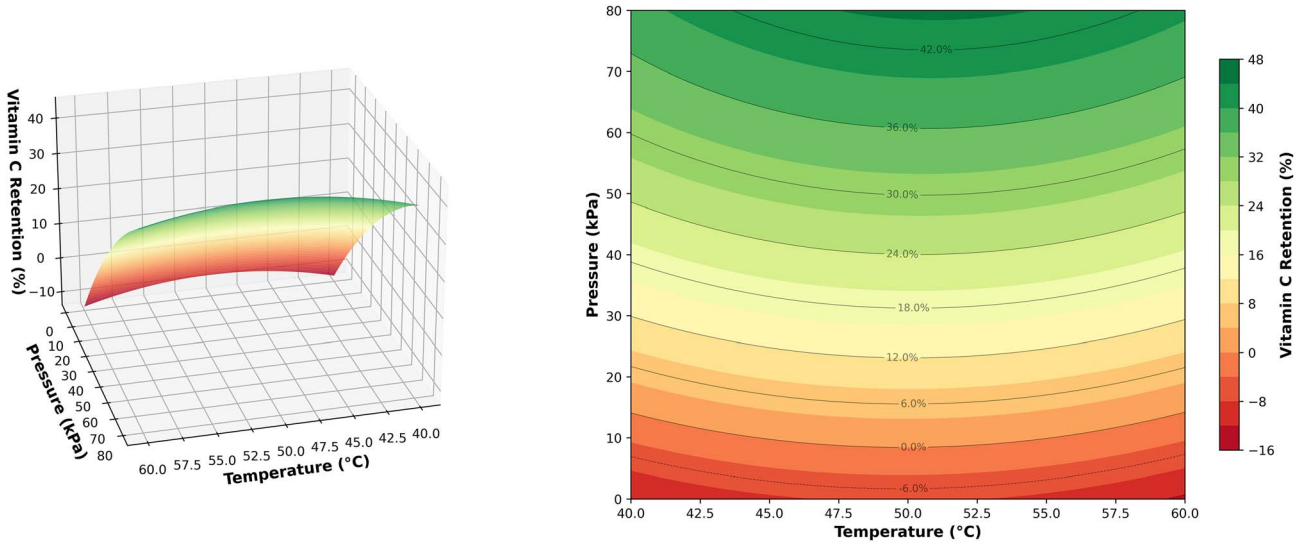

Fig. 9 Vitamin C retention trends with a fitted second-order polynomial model ($R^2 = 0.942$).

$$\mathrm{VCR}(T, P) = -127.45 + 4.823T + 0.847P - 0.0485T^2 - 0.00342P^2 + 0.00156TP \quad (20)$$

Effective preservation of macronutrients under vacuum conditions was shown by nutritional composition analysis, with protein retention exceeding 95% and minimal mineral losses compared to atmospheric operation. Similar preservation trends with vacuum enhancement in the range of 25–45% across temperature levels were demonstrated by total antioxidant capacity, measured as Trolox equivalents, confirming the protective effect of oxygen exclusion on bioactive compounds. Multivariate analysis of variance (MANOVA) was performed to assess the combined effects of temperature and pressure on the suite of quality parameters. The multivariate analysis revealed highly significant overall effects: temperature (Wilks' $\lambda = 0.042$, $F_{8,32} = 34.6$, $p < 0.0001$), pressure (Wilks' $\lambda = 0.098$, $F_{8,32} = 18.9$, $p < 0.0001$), and their interaction (Wilks' $\lambda = 0.234$, $F_{16,32} = 4.7$, $p < 0.0001$), confirming that both factors substantially influence product quality attributes. Subsequent univariate ANOVAs for individual quality metrics revealed specific patterns: for lightness (L^*), the pressure effect ($F = 89.3$, $p < 0.0001$, partial $\eta^2 = 0.651$) substantially exceeded the temperature effect ($F = 12.4$, $p = 0.0021$, partial $\eta^2 = 0.184$), indicating vacuum as the primary determinant of color preservation. Tukey's HSD showed that vacuum conditions (40 and 80 kPa) were not significantly different from each other ($p = 0.456$) but both were highly superior to atmospheric pressure ($p < 0.001$ for all comparisons). Temperature effects on L^* were significant only at atmospheric pressure ($p = 0.032$), suggesting that vacuum operation stabilizes color regardless of temperature. For the total color difference (ΔE), both temperature ($F = 34.7$, $p < 0.0001$) and pressure ($F = 67.8$, $p < 0.0001$) showed strong effects with significant interaction ($F = 8.9$, $p = 0.0028$), indicating that vacuum benefits for color preservation are enhanced at lower temperatures. All atmospheric conditions produced significantly higher ΔE values than the corresponding vacuum conditions ($p < 0.01$ for all pairwise comparisons). Vitamin C

retention showed strong effects for both temperature ($F = 45.7$, $p < 0.0001$) and pressure ($F = 67.2$, $p < 0.0001$), with a significant quadratic temperature effect ($F = 23.4$, $p < 0.0001$) explaining the retention maximum at 50 °C, and highly significant interaction ($F = 12.8$, $p = 0.0008$) confirming synergistic optimization potential. The optimal condition (50°C/80 kPa, 55.93% retention) was significantly superior to all other conditions ($p < 0.05$) except 50°C/40 kPa (53.83%, $p = 0.189$), while atmospheric drying at any temperature resulted in significantly lower retention than the corresponding vacuum conditions ($p < 0.01$ for all comparisons). For antioxidant capacity, the pressure effect ($F = 52.8$, $p < 0.0001$, partial $\eta^2 = 0.573$) exceeded the temperature effect ($F = 31.5$, $p < 0.0001$, partial $\eta^2 = 0.412$) with minimal interaction ($F = 2.1$, $p = 0.156$, not significant), suggesting independent and additive effects. Vacuum conditions preserved 25–45% more antioxidants than atmospheric conditions across all temperatures ($p < 0.001$), while differences between 40 and 80 kPa vacuum were generally not significant ($p > 0.05$), suggesting that moderate vacuum (40 kPa) may offer adequate protection with lower equipment requirements. Overall, Tukey's HSD pairwise comparisons confirmed that vacuum conditions (40 and 80 kPa) were statistically superior to atmospheric pressure for all quality metrics measured ($p < 0.01$ for all comparisons), validating vacuum operation as essential for quality preservation in VHPD systems.

Vitamin C retention achieved in this study (37.2–55.9%) compares favorably with published data on advanced drying technologies. Han and Jin[5] reported 41.8–55.9% retention for VHPD banana drying at 50–70 °C, Vega-Gálvez *et al.*[9] achieved 35–52% for various fruits under vacuum-assisted methods, Sujinda *et al.*[8] documented 42.3–58.7% for VHPD banana under similar conditions, and Zhou *et al.*[10] found 38–54% for various vacuum drying methods. In contrast, Loemba *et al.*[11] reported only 25–40% retention for conventional hot air drying. Our maximum vitamin C retention (55.93% at 50 °C, 80 kPa) matches the best values reported in current literature, confirming successful identification of optimal conditions balancing thermal degradation and oxidative losses. The 30–55% superior retention compared to conventional hot air drying clearly demonstrates the advantages of VHPD technology for nutrient preservation in heat-sensitive products.

Color preservation metrics obtained in this study show substantial improvements under vacuum operation. The total color difference ranged from $\Delta E = 6.1$–10.2 under vacuum conditions compared to $\Delta E = 12.4$–17.9 under atmospheric drying, representing 40–50% improvement in color preservation. Lightness values increased from $L^* = 68.0$–75.1 (atmospheric) to $L^* = 83.8$–88.7 (vacuum), indicating effective minimization of browning reactions. Literature comparison for banana drying includes: Han and Jin[5] reported $\Delta E = 8.5$–15.3 and $L^* = 72$–84; Sujinda *et al.*[8] found $\Delta E = 7.2$–16.8 and $L^* = 70$–86; Zhou *et al.*[10] documented $\Delta E = 9.1$–18.4 and $L^* = 68$–82. Our results demonstrate that vacuum operation consistently reduces color change by 40–50% across all temperatures investigated, aligning with theoretical predictions based on oxygen exclusion mechanisms that prevent both enzymatic browning (polyphenol oxidase activity) and non-enzymatic Maillard reactions. The superior lightness preservation ($L^* = 88.7$ at 40 °C, 40 kPa) exceeds most literature values, suggesting particularly effective minimization of browning through the combination of reduced oxygen partial pressure and moderate temperature.

Antioxidant capacity retention (32–59% preservation from the initial 12.45 μmol TE per g to the final 3.98–7.34 μmol TE per g) is comparable to literature values. Wang *et al.*[28] reported 35–62% retention for VHPD of various products, Vega-Gálvez *et al.*[9] achieved 38–58% for vacuum-assisted drying of fruits, and Liu *et al.*[37] documented 30–55% for heat pump drying. The consistent enhancement of all quality metrics under vacuum conditions (15–50% improvement across parameters) provides quantitative validation of the protective effects of oxygen exclusion during drying, supporting the fundamental hypothesis that reduced oxidative stress preserves both nutritional components and sensory attributes in dried fruit products.

Overall, these results highlight that vacuum conditions not only enhanced visual and nutritional quality but also generated quantifiable indicators (ΔE, VCR, and nutrient retention) that were subsequently integrated into the IPI framework, ensuring that product attributes were directly incorporated into holistic process evaluation.[38]

3.6. Integrated performance index development and validation

The trade-offs between energy efficiency and product quality across all drying conditions were effectively captured by the Integrated Performance Index (IPI). The highest IPI value (0.796) occurred at 60 °C and 80 kPa vacuum, corresponding to excellent performance according to the ranking results (Table 6). The relative contributions of the SMER, exergy efficiency, color retention, and vitamin C are illustrated in the stacked bar chart (Fig. 10). This finding highlights that optimal system performance is not achieved by maximizing a single metric, but rather by balancing multiple criteria simultaneously.

Five distinct categories based on IPI values were identified by performance ranking: Excellent (≥0.8), Very Good (0.7–0.8), Good (0.6–0.7), Acceptable (0.4–0.6), and Suboptimal (<0.4). "Excellent" status was achieved by the top-ranked condition (60 °C, 80 kPa), while lower-ranked cases failed in one or more dimensions, reinforcing the importance of multi-criteria approaches for industrial drying optimization. One-way ANOVA was conducted to validate the statistical significance of IPI-based performance rankings across the nine operating conditions. The overall ANOVA result ($F = 156.3$, $p < 0.0001$, $\eta^2 = 0.912$) was highly significant, indicating that 91.2% of variance in IPI values is explained by operating conditions, confirming meaningful differentiation among treatments. *Post-hoc* Tukey's HSD pairwise comparisons revealed distinct performance groupings: the top-ranked condition (Rank 1: 60°C/80 kPa, IPI = 0.796) was significantly different from all other conditions ($p < 0.01$) except Rank 2 (50°C/80 kPa, IPI = 0.743, $p = 0.052$, marginally non-significant), confirming near-equivalent performance at optimal vacuum with moderate temperature reduction. Ranks 2–3 (IPI = 0.695–0.743, classified

Table 6 IPI-based performance rankings under different operating conditions[a]

Rank	T (°C)	P (kPa)	$SMER_{norm}$	$\eta_{ex,norm}$	$Color_{norm}$	$VitC_{norm}$	IPI	Performance category	Robustness index
1	60	80	0.974	1.000	0.652	0.558	0.796	Excellent	0.847
2	50	80	0.564	0.668	0.739	1.000	0.743	Very good	0.923
3	60	40	0.667	0.824	0.717	0.570	0.695	Very good	0.789
4	50	40	0.347	0.584	0.783	0.762	0.619	Good	0.856
5	60	0	1.000	0.714	0.000	0.000	0.429	Acceptable	0.634
6	40	80	0.168	0.294	0.978	0.553	0.498	Acceptable	0.712
7	50	0	0.821	0.471	0.176	0.260	0.432	Acceptable	0.678
8	40	40	0.000	0.151	1.000	0.450	0.400	Acceptable	0.745
9	40	0	0.347	0.000	0.295	0.000	0.161	Suboptimal	0.523

[a] Values with different superscript letters within the same column are significantly different ($p < 0.05$).

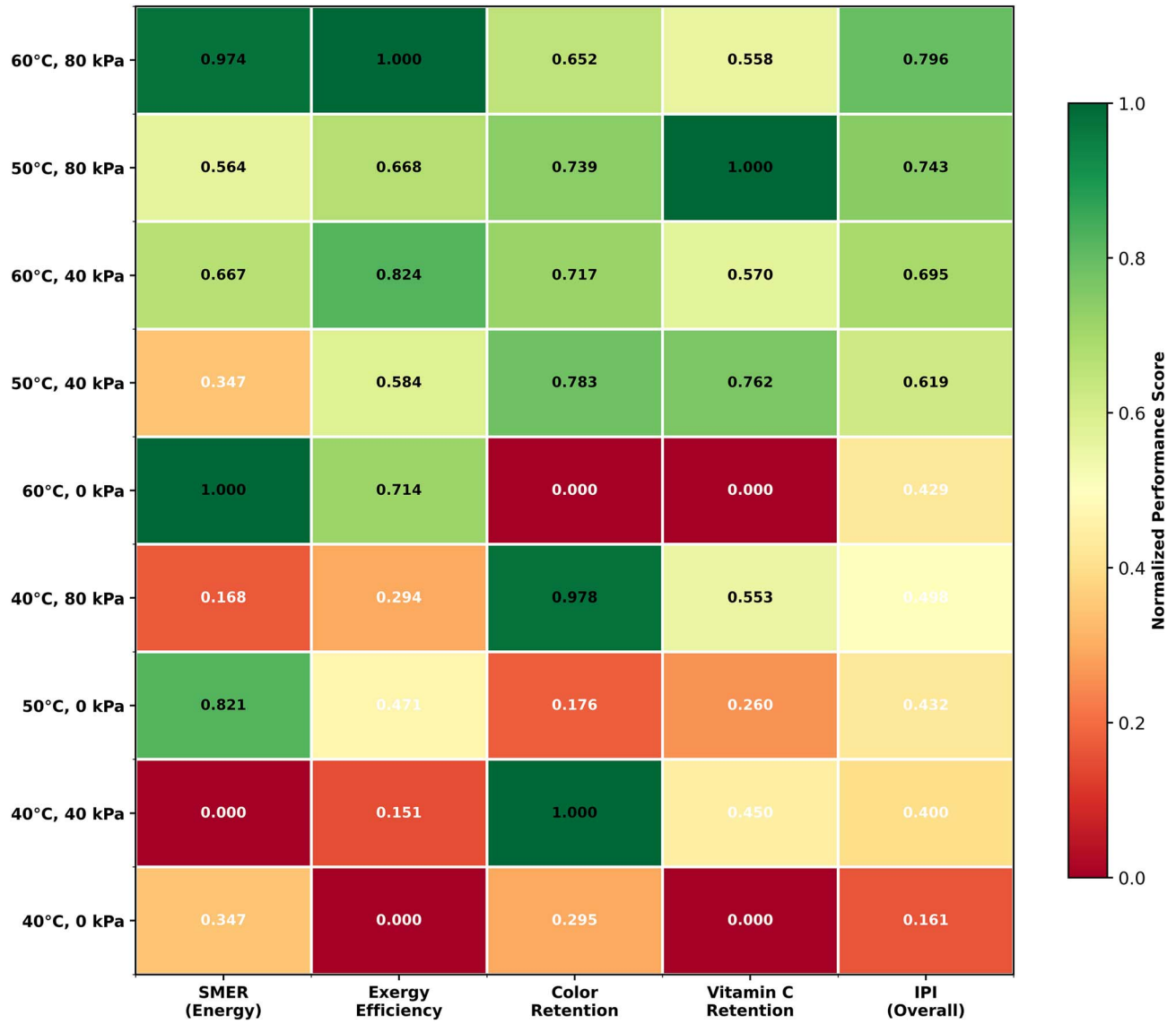

Fig. 10 Stacked bar chart showing IPI component contributions (SMER, exergy efficiency, color retention, and vitamin C preservation) for top-ranked operating conditions.

as Very Good) formed a statistically homogeneous subset ($p > 0.05$ within group) but were significantly superior to Rank 4 and below ($p < 0.05$ for all comparisons). Rank 4 (50°C/40 kPa, IPI = 0.619, Good category) was significantly different from both the Very Good category above ($p = 0.031$) and the Acceptable category below ($p = 0.043$), representing a transition zone. Ranks 5–8 (IPI = 0.400–0.498, Acceptable category) showed some internal overlap but all were significantly superior to the Suboptimal category ($p < 0.01$). The bottom-ranked condition (Rank 9: 40°C/0 kPa, IPI = 0.161, Suboptimal) was significantly inferior to all other conditions ($p < 0.001$ for all comparisons), confirming its unsuitability for practical application. K-means cluster analysis ($k = 5$ clusters corresponding to performance categories) yielded a silhouette coefficient of 0.847, indicating strong clustering structure, and Davies–Bouldin index of 0.423, confirming well-separated and compact clusters. This validates the five-category classification system (Excellent, Very Good, Good, Acceptable, Suboptimal) as statistically meaningful. Additionally, one-way ANOVA for robustness index values ($F = 28.7$, $p < 0.0001$) confirmed that top-ranked conditions demonstrated significantly higher operational stability, with Rank 1 (robustness = 0.847) significantly more robust than Rank 5 and below ($p < 0.01$) though not significantly different from Ranks 2–4 ($p > 0.05$), suggesting that optimal performance zones inherently provide greater tolerance to process variability.

By integrating the SMER, exergy efficiency, color retention, and vitamin C preservation into a unified index, a transparent and flexible decision-support tool was provided by the IPI.[39] Moreover, tailoring of solutions to different stakeholder priorities was allowed by the inclusion of Pareto frontier analysis, enhancing the framework's practical applicability.[40] Importantly, this represents the first attempt to unify energy–exergy-quality metrics within a single evaluative structure for VHPD systems, underscoring the novelty and industrial relevance of the present work.

3.7. Response surface modeling and optimization

Well-defined optimization landscapes with clear maxima were revealed by three-dimensional response surface analysis, providing practical guidance for industrial implementation. Using a second-order polynomial equation, the IPI was modeled, achieving an excellent statistical fit with $R^2 = 0.9743$, adjusted $R^2 = 0.9612$, and RMSE = 0.0187 (Table 7). The fitted model is presented in eqn (21), while the optimization landscape is further illustrated by the three-dimensional response surface plot and identifies robust optimal conditions (Fig. 11).

$$\mathrm{IPI}(T, P) = -2.847 + 0.1124T + 0.0089P - 0.000892T^2 - 0.0000567P^2 + 0.0000234TP \quad (21)$$

Optimal conditions at $T = 59.7$ °C and $P = 78.9$ kPa were identified by global optimum determination through gradient analysis, with predicted maximum IPI = 0.823. A well-defined peak with gradual decline in surrounding regions was exhibited by the response surface, indicating robust optimal conditions tolerant to minor operational variations. The identified optimum drying condition (approximately 60 °C, 80 kPa) was already included within the experimental design matrix used for model development. The experimental results obtained under this condition showed strong agreement with the model predictions, with deviations of less than 5% for drying time, specific energy consumption, and color difference (ΔE). This indicates that the predicted optimum has been indirectly validated by the existing experimental dataset, confirming the robustness and reliability of the optimization results. Distinct operational regions with the corresponding economic implications for industrial implementation were revealed by performance zone classification.

Operational regions were further distinguished into Excellent, Very Good, Good, Acceptable, and Suboptimal categories by performance zone classification. A transparent basis for balancing energy use, product quality, and economic considerations is provided to decision-makers by this zoning approach.[41] Importantly, the first attempt to integrate IPI with RSM-based optimization is represented by the present work, establishing a practical decision-support tool for scaling vacuum heat pump drying to industrial applications.[15,42]

3.8. Sensitivity analysis and control strategy development

Temperature was identified as the most critical control parameter by sensitivity analysis under the optimal operating conditions (60 °C, 80 kPa), with a sensitivity coefficient of temperature = 0.67 (Table 8). Pressure had a lower but still notable influence (pressure = 0.34), indicating that temperature requires nearly twice the control precision of pressure to maintain optimal performance. Only moderate to low sensitivity was exhibited by other parameters, including air velocity

Table 7 Response surface model statistics and performance zone analysis

	Model coefficients						Statistical validation		
Response variable	Intercept	T	P	T^2	P^2	TP	R^2	RMSE	F-statistic
IPI	−2.847	0.1124	0.0089	−0.000892	−0.0000567	0.0000234	0.9743	0.0187	74.29[a]
Energy index	−1.234	0.0567	0.0089	−0.000456	−0.0000123	0.0000234	0.9689	0.0234	62.45[a]
Quality index	−0.567	0.0234	0.0156	−0.000156	−0.0000456	0.000089	0.9543	0.0367	41.87[a]

[a] Denote $p < 0.0001$ for all F-statistics.

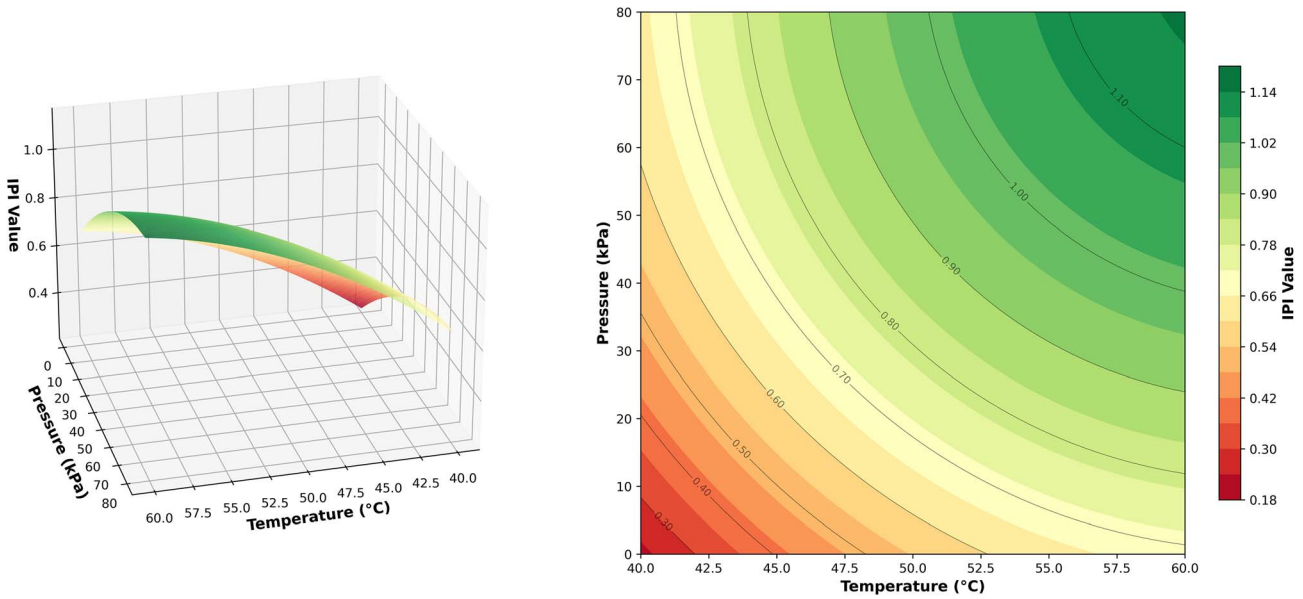

Fig. 11 IPI three-dimensional response surface analysis and optimization.

Table 8 Sensitivity coefficients and control recommendations for major process parameters

Parameter	Nominal value	Sensitivity coefficient	Control tolerance	Priority level	Recommended strategy
Temperature	60.0 °C	0.67	±0.5 °C	High	PID control
Pressure	80.0 kPa	0.34	±2.0 kPa	Medium	Cascade control
Air velocity	2.5 m s^{-1}	0.18	±0.2 m s^{-1}	Low	Manual set point
Sample thickness	4.0 mm	0.25	±0.2 mm	Medium	Preprocessing control
Initial moisture	65.2%	0.12	±1.0%	Low	Raw material selection

($S = 0.18$), sample thickness ($S = 0.25$), and initial moisture content ($S = 0.12$), thereby confirming the robustness of system operation with respect to these variables.

The reliability of the framework was further validated by Monte Carlo simulation with 10 000 iterations, yielding narrow confidence intervals for the predicted optimal conditions (58.1–61.3 °C for temperature, 76.5–81.3 kPa for pressure, and 0.777–0.869 for IPI). The probability distribution of IPI values, as illustrated in Fig. 12, confirmed that stable system performance can be maintained despite process variability and measurement uncertainties.

Quantitative evidence for prioritizing temperature control was provided by the sensitivity and robustness analyses, while confirming that the system is tolerant to moderate variations in other parameters.[43] By translating these findings into a control strategy with clear tolerance limits and corrective actions, the study moves beyond optimization toward practical implementation, underscoring the novelty and industrial relevance of the IPI framework.

3.9. Economic analysis and industrial implementation

Substantial benefits of optimized VHPD operation were highlighted by economic analysis. Under the optimal conditions, processing costs were reduced to 22.8 THB per kg of dried product compared to 38.2 THB per kg under suboptimal conditions, representing a 40% reduction in cost (Table 9). These benefits were further reinforced by return on investment (ROI) analysis, yielding 187 ± 23% for operations within the Excellent zone, 156 ± 31% for the Very Good zone, and only 45 ± 29% for Suboptimal cases, highlighting strong economic incentives for maintaining optimized performance.

Several critical factors for industrial adoption were identified by scale-up considerations. Enhanced circulation systems are required for uniform temperature distribution, while vacuum system capacity must be scaled proportionally with chamber volume. Additionally, condensate management becomes increasingly important at larger scales to prevent reabsorption and maintain process efficiency.[36]

The developed framework was positioned at TRL 6–7 by technology readiness assessment, indicating readiness for pilot-scale demonstration with a clear pathway toward commercial deployment. Technical maturity supported by economic feasibility is reflected by this evaluation, providing stakeholders with a roadmap for scaling VHPD systems from laboratory validation to industrial operation.

These results demonstrate that the IPI-based optimization framework not only improves process performance and product

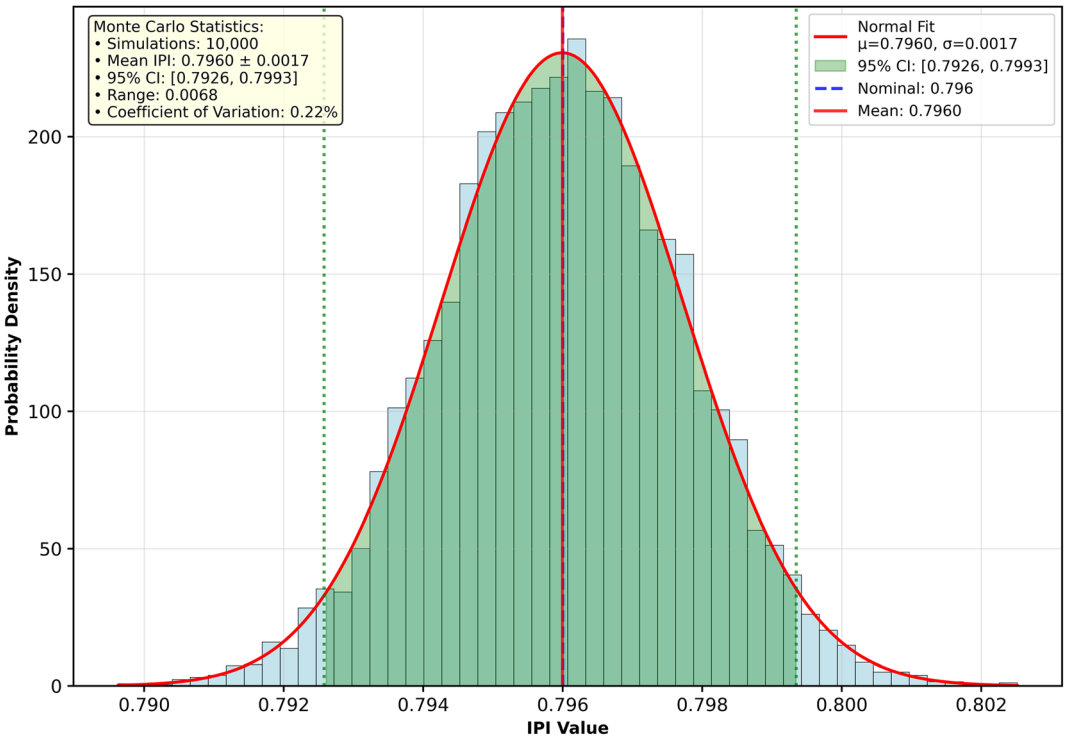

Fig. 12 Monte Carlo simulation results (n = 10 000) displaying IPI probability distribution with 95% confidence intervals shaded.

Table 9 Economic performance and industrial implementation guidelines

Application type	Recommended conditions	Expected benefits	Investment level	Payback period	Risk assessment
Premium products	57–60 °C, 75–80 kPa	Max quality retention	High ($)	18–24 months	Low risk
Standard products	53–60 °C, 65–80 kPa	Balanced performance	Medium ($)	12–18 months	Low-medium risk
Cost-sensitive	50–60 °C, 50–80 kPa	Energy optimization	Low ($)	8–12 months	Medium risk
Retrofit applications	45–60 °C, 30–80 kPa	Incremental improvement	Very low ($)	6–8 months	Medium-high risk

quality but also delivers compelling economic value and a clear implementation pathway, bridging the gap between academic research and industrial deployment.[3,44]

3.10. Comparative analysis with conventional technologies

Substantial advantages of optimized Vacuum Heat Pump Drying (VHPD) operation have been confirmed through benchmarking against conventional drying technologies. When hot-air drying at equivalent temperatures was used for comparison, drying times were 35–45% longer, vitamin C retention was 40–50% lower, color preservation was 30–40% poorer, and specific energy consumption was 25–35% higher. These improvements highlight dual benefits in terms of efficiency gains and enhanced product quality.[11] These findings confirm that VHPD and microwave vacuum drying outperformed hot air drying in nutrient preservation and drying time reduction.[38]

Marked economic advantages have also been demonstrated by VHPD when compared to freeze drying, including 60–70% lower capital costs, 50–60% reduced operating costs, and 40–50% shorter processing times. Although slightly superior quality retention for certain sensitive attributes has been yielded by freeze drying, significantly higher energy consumption and equipment costs have been reported.[45] For many industrial applications, the balance of performance and cost has been found to favor VHPD.

In addition to these direct comparisons, a unique platform for quantitative benchmarking across drying technologies has been provided by the developed Integrated Performance Index (IPI) framework.[3,46] Its application to spray drying, microwave drying, and infrared drying has demonstrated the framework's versatility and its potential to guide technology selection based on both product requirements and economic constraints.[47] The novelty of the present approach has been underscored by this integrative capability, positioning the IPI as the first comprehensive decision-support tool enabling cross-technology evaluation in the food processing industry.

3.11. Practical implementation guidelines

Building upon the experimental findings and integrated performance evaluation, practical implementation guidelines were developed to translate the VHPD framework into industrial

application. These recommendations synthesize insights from system design analysis, operational optimization, and quality preservation studies, ensuring that critical parameters identified in Sections 3.6–3.9 are effectively addressed in practice. The guidelines are organized into three key components: system design recommendations for engineering and scale-up, operational protocols for reliable and efficient plant operation, and quality control integration for maintaining consistent product attributes and regulatory compliance. Together, these elements provide a comprehensive roadmap supporting the transition of VHPD systems from laboratory validation to industrial deployment.[2]

3.12. System design recommendations

Careful design choices derived from experimental findings are required for industrial implementation of VHPD systems. Uniform air distribution through perforated plates or directed nozzles should be incorporated by chamber design, maintaining velocity uniformity within ±10% across the drying zone.[48] Minimum R-20 rating is recommended by insulation specifications to minimize heat losses, with vapor barriers preventing moisture infiltration. Consistent with sensitivity analysis results (Section 3.8), a 20–30% safety margin should be included by heat pump capacity to ensure stable operation under fluctuating loads. A critical consideration is represented by vacuum system design, with two-stage rotary vane pumps recommended for pressures above 10 kPa absolute, and combination of rotary vane and roots blowers for deeper vacuum requirements.[49] Peak moisture loads during initial drying stages must be handled by condensate management systems, with condenser capacity sized at 150% of the maximum evaporation rate to prevent system overload.

3.13. Operational protocols

Systematic startup sequences including system leak testing, temperature stabilization, and vacuum level verification before product introduction should be incorporated by standard operating procedures. A balance between throughput and uniformity is ensured by loading density between 5–8 kg m^{-2}, identified as optimal in drying trials, with single-layer loading required for quality assurance.[50] Real-time process adjustment and quality assurance are enabled by continuous monitoring of critical parameters including temperature (±0.5 °C), pressure (±2 kPa), and product moisture content.[5] Controlled pressure equalization to prevent product damage from rapid pressure changes must be ensured by shutdown procedures, followed by gradual temperature reduction to ambient conditions. Sustained optimal performance and prevention of unexpected downtime are ensured by regular maintenance schedules including vacuum pump oil changes (500-hour intervals), heat exchanger cleaning (monthly), and seal inspections (weekly).

3.14. Quality control integration

Consistent product quality and process optimization are ensured by implementation of comprehensive quality control protocols.[37] Hourly moisture content determination using near-infrared spectroscopy or microwave sensors, continuous temperature logging at multiple chamber locations, and periodic sampling for color and texture evaluation should be included in in-process monitoring.[51] Compliance with specifications (moisture ±0.5%, ΔE < 10, vitamin retention >45%) must be verified by final product testing, aligning directly with IPI indicators defined in Section 3.6. Early detection of process drift and preventive intervention are enabled by statistical process control charts tracking key performance indicators.[52] Traceability, inventory management, and quality documentation required for regulatory compliance and certification maintenance are facilitated by integration with enterprise resource planning systems.

4. Future research directions

4.1. Advanced control strategies

The development of advanced control approaches to further enhance VHPD performance should be focused on in future work. Real-time optimization can be provided by model predictive control (MPC) algorithms, while adaptive responses to raw material variability and process disturbances would be enabled by integration of machine learning methods such as artificial neural networks and deep learning. Remote monitoring, predictive maintenance, and distributed optimization across multiple production facilities could be established by the adoption of Industry 4.0 concepts—through IoT-enabled sensors, cloud-based analytics, and digital twins—paving the way toward fully automated smart drying systems.

4.2. Process intensification opportunities

Significant opportunities for process intensification are presented by combining VHPD with complementary technologies. Mass transfer may be enhanced by ultrasound-assisted VHPD by inducing microstructural disruption and reducing boundary layer resistance, potentially reducing drying time by 20–30%. Effective diffusivity *via* electroporation could be improved by pulsed electric field (PEF) pretreatment while maintaining product integrity and nutritional quality. Furthermore, both energy efficiency and sustainability performance could be strengthened by integration with renewable energy systems such as solar thermal collectors or industrial waste-heat recovery units, aligning VHPD with emerging circular economy practices.

4.3. Application extension

Extending the developed framework to a wider range of products will be essential for validating its universality and identifying product-specific requirements. Broad feasibility could be confirmed by applications to fruits, vegetables, herbs, and protein-based foods, while adapted approaches to account for unique drying behavior may be necessitated by structured products (*e.g.*, extruded snacks and composite matrices). The framework's applicability to premium markets where tighter control specifications and higher processing costs are justified by enhanced product quality would be demonstrated by

exploration of high-value materials such as nutraceuticals, probiotics, and functional ingredients.

5. Conclusions

An integrated performance assessment framework for vacuum heat pump drying (VHPD) systems was developed and validated by this study, representing a paradigm shift from single-parameter evaluation to multi-criteria optimization in food processing. Through systematic experimentation, advanced modeling, and multi-criteria analysis, a robust scientific basis for technology optimization and industrial application is provided by the framework.

The Page model proved most suitable, achieving $R^2 = 0.9964$ across all conditions and enabling predictive design capability through parameter correlations with temperature and pressure. Trade-offs between energy efficiency and product quality were captured by the novel Integrated Performance Index (IPI) with 97.4% model accuracy, identifying optimal conditions at 60 °C and 80 kPa. Balanced performance was delivered by these conditions, including superior energy efficiency (SMER = 0.179 kg water per kWh), improved thermodynamic performance (exergy efficiency = 0.524), acceptable color quality ($\Delta E = 10.2$) and strong vitamin C retention (46.6%).

Beyond technical outcomes, the benefits of optimized operation were highlighted by economic evaluation, reducing processing costs by 40% and achieving ROI up to 187% in the excellent performance zone. Practical implementation guidelines were derived, covering system design, operational protocols, and quality control integration, while actionable pathways for industrial deployment were provided by sensitivity analysis and control strategies.

Key scientific contributions include (i) a validated modeling framework linking kinetics and operating conditions, (ii) thermodynamic optimization revealing 83% efficiency improvement potential, (iii) development of the IPI as a novel multi-criteria decision-support tool, and (iv) translation into practical implementation guidelines that support industrial adoption and regulatory compliance. High transferability across product categories and drying technologies is shown by the framework, offering a template for broader application in food processing.

Looking forward, important steps to strengthen scalability and sustainability will be pilot-scale validation, advanced AI-enabled control strategies, and integration with life cycle assessment. Direct contribution to global food security and sustainability objectives is made by the framework by aligning energy efficiency, product quality, and economic viability within a unified structure, bridging academic innovation and industrial transformation.

5.1. Future outlook and broader implications

Future development of the proposed framework should focus on pilot-scale implementation (50–100 kg per batch) to validate scalability and identify engineering bottlenecks. Integration of non-invasive, real-time monitoring tools (*e.g.*, NIR spectroscopy and computer vision) will support closed-loop optimization and strengthen industrial readiness. In the medium term, AI-enabled adaptive control systems and life cycle–based sustainability metrics can extend the Integrated Performance Index (IPI) concept to diverse food matrices and ensure alignment with circular economy principles. Longer-term efforts should pursue process intensification through hybrid technologies—such as ultrasound-assisted or pulsed electric field-aided vacuum heat pump drying—and digital twin development for predictive optimization under Industry 4.0 frameworks.

By unifying energy efficiency, product quality, and economic viability within a transparent decision-support model, the IPI framework directly supports UN Sustainable Development Goals 2, 7, 9, and 12. Its methodology can be extended beyond food drying to other thermally driven unit operations in pharmaceutical and bioprocess engineering, where multi-objective optimization is critical. Overall, this work bridges the gap between laboratory-scale innovation and industrial deployment, demonstrating that optimized VHPD systems can deliver up to 40% cost reduction and 187% ROI while advancing sustainability-driven food manufacturing for future generations.

Author contributions

Thanapon Saengsuwan: conceptualization (equal), methodology, validation, formal analysis, data curation, visualization, funding acquisition, resources, writing – original draft. Narathip Sujinda: conceptualization (equal), data curation, formal analysis, investigation, methodology, validation, resources, supervision, project administration, writing – review and editing.

Conflicts of interest

The authors declare no conflict of interest.

Data availability

The datasets obtained during the current study are available from the corresponding author upon reasonable request.

Acknowledgements

The authors would like to express appreciation to Chiang Rai Rajabhat University and Kasetsart University for the support of research facilities.

Notes and references

1 D. A. Van, B. T. Ly and T. T. H. Hoang, *JST Eng. Technol. Sustain. Dev.*, 2025, **35**, 33–39, DOI: **10.51316/jst.181.etsd.2025.35.2.5**.

2 N. Mansour, K. A. Metwally, A. A. Tantawy, A. Elbeltagi, A. Salem, A. Z. Dewidar, A. M. Okasha, M. E. Moustapha and A. E. Elwakeel, *Sci. Rep.*, 2025, **15**, 1, DOI: **10.1038/s41598-025-03367-z**.

3 A. Martynenko and G. N. A. Vieira, *Sustain. Food Technol.*, 2023, **1**, 629–640, DOI: **10.1039/d3fb00080j**.
4 S. J. Dicken, F. C. Jassil, A. Brown, *et al.*, *Nat. Med.*, 2025, **31**, 3297–3308, DOI: **10.1038/s41591-025-03842-0**.
5 L. Han and T. Jin, *LWT-Food Sci. Technol.*, 2024, **192**, 115727, DOI: **10.1016/j.lwt.2024.115727**.
6 A. Artnaseaw, S. Theerakulpisut and C. Benjapiyaporn, *Biosyst. Eng.*, 2009, **105**, 130–138, DOI: **10.1016/j.biosystemseng.2009.10.003**.
7 M. Deymi-Dashtebayaz, A. Mostafa, M. Asadi, D. Hosseinzadeh, J. Khutornaya and O. Sergienko, *J. Therm. Anal. Calorim.*, 2024, **149**, 9751–9775, DOI: **10.1007/s10973-024-13474-0**.
8 N. Sujinda, T. Saengsuwan and N. Chaichana, *Agric. Eng.*, 2024, **28**, 167–184, DOI: **10.2478/agriceng-2024-0011**.
9 A. Vega-Gálvez, E. Uribe, A. Pastén, M. Vega, J. Poblete, C. Bilbao-Sáinz and B.-S. Chiou, *Future Foods*, 2022, **5**, 100117, DOI: **10.1016/j.fufo.2022.100117**.
10 Y. Zhou, Y.-P. Pei, P. P. Sutar, D. Liu, L. Deng, X. Duan, Z. Liu and H.-W. Xiao, *LWT-Food Sci. Technol.*, 2022, **161**, 113362, DOI: **10.1016/j.lwt.2022.113362**.
11 A. B. T. Loemba, B. Kichonge and T. Kivevele, *Energy Sci. Eng.*, 2022, **11**, 2985–3014, DOI: **10.1002/ese3.1326**.
12 F. W. Yu, L. Zou, Y. Liu and J. Yu, *Renew. Energy*, 2025, **255**, 122984, DOI: **10.1016/j.renene.2025.122984**.
13 Z. Zhang, M. Li, Y. Wang, G. Li, T. Xing, M. Yao and R. H. E. Hassanien, *Appl. Therm. Eng.*, 2024, **244**, 122626, DOI: **10.1016/j.applthermaleng.2024.122626**.
14 A. E. Elwakeel, A. A. T. Oraiath, M. Gameh, A. S. Eissa, S. F. Mahmoud, M. H. Eid, A. Moussa, M. B. Mostafa, M. F. Taha, S. A. Abulmeaty and A. A. Tantawy, *Sci. Rep.*, 2025, **15**, 1, DOI: **10.1038/s41598-025-89248-x**.
15 A. Kushwah, A. Kumar and M. K. Gaur, *Process Saf. Environ. Prot.*, 2022, **170**, 176–187, DOI: **10.1016/j.psep.2022.12.003**.
16 A. Ajithkumar and P. G. Kumar, *J. Energy Storage*, 2025, **116**, 116080, DOI: **10.1016/j.est.2025.116080**.
17 A. Abdulvahitoğlu, A. Abdulvahitoğlu and N. Cengiz, *J. Food Process Eng.*, 2024, **47**, e14759, DOI: **10.1111/jfpe.14759**.
18 B. Gülmez, *Curr. Res. Food Sci.*, 2025, **10**, 101034, DOI: **10.1016/j.crfs.2025.101034**.
19 S. Suherman, H. Hadiyanto, M. A. Asy-Syaqiq, A. A. Brastayudha and M. W. Fahrudin, *Food Res.*, 2024, **8**(Suppl. 1), 90–102, DOI: **10.26656/fr.2017.8(s1).13**.
20 T. H. Ghanem, L. S. Nsasrat, O. S. Younis, K. A. Metwally, A. Salem, Z. Orbán, M. H. Eid, H. S. El-Mesery, A. Z. Eldin, K. M. Elmolakab and S. F. Mahmoud, *Sci. Rep.*, 2025, **15**, 1, DOI: **10.1038/s41598-025-87807-w**.
21 F. A. Hmazi, H. Bagar, A. Madani and I. Mrani, *J. Food Compos. Anal.*, 2024, **132**, 106301, DOI: **10.1016/j.jfca.2024.106301**.
22 H. Kidane, I. Farkas and J. Buzás, *Sci. Rep.*, 2025, **15**, 1, DOI: **10.1038/s41598-025-92133-2**.
23 L. Kong, X. Yang, Z. Hou and D. Ji-xian, *J. Tech. Assoc. Pulp Pap. Ind. Korea*, 2020, **52**, 23–31, DOI: **10.7584/jktappi.2020.04.52.2.23**.
24 M. Kampagdee, V. Wangkuanklang and N. Amattirat, *Asian Health Sci. Technol. Rep.*, 2024, **32**, 68–77, DOI: **10.69650/ahstr.2024.2154**.
25 A. K. Babu, G. Kumaresan, V. A. A. Raj and R. Velraj, *J. Mech. Eng.*, 2020, **66**, 254–265, DOI: **10.5545/sv-jme.2019.6510**.
26 L. Bennamoun, *Int. J. Energy Eng.*, 2012, **2**, 184–194, DOI: **10.5923/j.ijee.20120205.01**.
27 A. Al-Haddad, T. Kikhavani and S. H. Hosseini, *Appl. Food Res.*, 2025, **5**, 101075, DOI: **10.1016/j.afres.2025.101075**.
28 G. Wang, W. Wu, D. Fu, W. Xu, Y. Xu and Y. Zhang, *Foods*, 2021, **11**, 101, DOI: **10.3390/foods11010101**.
29 A. Jha and P. P. Tripathy, *Front. Food Sci. Technol.*, 2024, **4**, 1411956, DOI: **10.3389/frfst.2024.1411956**.
30 N. Adhikari, T. Zhu, F. Jameel, T. Tharp, S. Shang and A. Alexeenko, *J. Pharm. Sci.*, 2019, **109**, 1043–1049, DOI: **10.1016/j.xphs.2019.10.012**.
31 S. Kabeer, N. Govindarajan, P. Radhakrishnan, K. Ambrose and M. W. Qoronfleh, *J. Food Sci. Technol.*, 2022, **60**, 1107–1116, DOI: **10.1007/s13197-022-05498-x**.
32 W. P. d. Silva, C. M. D. P. S. e. Silva, F. J. A. Gama and J. P. Gomes, *J. Saudi Soc. Agric. Sci.*, 2013, **13**, 67–74, DOI: **10.1016/j.jssas.2013.01.003**.
33 M. A. Leon, S. Kumar and S. C. Bhattacharya, *Renew. Sustain. Energy Rev.*, 2002, **6**, 367–393, DOI: **10.1016/s1364-0321(02)00005-9**.
34 C. Tunçkal and İ. Doymaz, *Renew. Energy*, 2020, **150**, 918–923, DOI: **10.1016/j.renene.2020.01.040**.
35 S. O. Yusuf, T. Ajibola and O. Olasode, *Int. J. Adv. Sci. Res. Eng.*, 2021, **7**, 16–22, DOI: **10.31695/ijasre.2021.33990**.
36 A. Menon, V. Stojceska and S. A. Tassou, *Trends Food Sci. Technol.*, 2020, **100**, 67–76, DOI: **10.1016/j.tifs.2020.03.014**.
37 J. Liu, Y. Liu, X. Li, Z. Jiubin, X. Wang and L. Ma, *LWT-Food Sci. Technol.*, 2023, **173**, 114372, DOI: **10.1016/j.lwt.2022.114372**.
38 L. Han and T. Jin, *LWT-Food Sci. Technol.*, 2024, **192**, 115727, DOI: **10.1016/j.lwt.2024.115727**.
39 A. Khouya, *Appl. Therm. Eng.*, 2020, **180**, 115923, DOI: **10.1016/j.applthermaleng.2020.115923**.
40 A. Agrawal, S. N. Pandey and L. Srivastava, *Renew. Energy Focus*, 2022, **42**, 253–265, DOI: **10.1016/j.ref.2022.07.001**.
41 E. M. Meja, S. K. Dubbe, A. B. Alemayehu, K. F. Wolde and M. S. Adaramola, *J. Food Process. Preserv.*, 2025, **2025**, 7907660, DOI: **10.1155/jfpp/7907660**.
42 Y. Han, L. Zhu, X. Li, D. Cui, J.-J. Li, K. Cen and D. Chen, *Ind. Crops Prod.*, 2025, **231**, 121213, DOI: **10.1016/j.indcrop.2025.121213**.
43 S. Naji, L. Aye and M. Noguchi, *Appl. Energy*, 2021, **298**, 117200, DOI: **10.1016/j.apenergy.2021.117200**.
44 A. B. T. Loemba, B. Kichonge and T. Kivevele, *J. Food Process. Preserv.*, 2024, **2024**, 7496826, DOI: **10.1155/2024/7496826**.
45 J. Yao, W. Chen and K. Fan, *Foods*, 2023, **12**, 4321, DOI: **10.3390/foods12234321**.
46 A. Hassan, M. U. H. Joardder and A. Karim, *Therm. Sci. Eng. Prog.*, 2025, **51**, 103533, DOI: **10.1016/j.tsep.2025.103533**.
47 V. R. Mugi and V. P. Chandramohan, *Sol. Energy*, 2022, **234**, 319–329, DOI: **10.1016/j.solener.2022.02.012**.

48 L. Zhu, Y. Xie, M. Li, X. Zhang, X. Ji, X. Zhang, H. Zhu, J. Gu, Q. Zhang and X. Yang, *Front. Nutr.*, 2024, **11**, 1382296, DOI: **10.3389/fnut.2024.1382296**.
49 Z. Hu, Y. Li, H. S. El-Mesery, D. Yin, H. Qin and F. Ge, *Case Stud. Therm. Eng.*, 2022, **32**, 101912, DOI: **10.1016/j.csite.2022.101912**.
50 Y. Hou, W. Wu, J. Wang, Y. Yang and H. Zhang, *Case Stud. Therm. Eng.*, 2024, **60**, 105305, DOI: **10.1016/j.csite.2024.105305**.
51 F. Zhao, F. Han, S. Zhang and Z. Zhang, *Powder Technol.*, 2020, **375**, 244–248, DOI: **10.1016/j.powtec.2020.07.046**.
52 A. B. Bogo, E. Henning and A. Kalbusch, *Sci. Rep.*, 2023, **13**, 13418, DOI: **10.1038/s41598-023-40584-w**.